Resource

Molecular Cell

Programmable Inhibition and Detection of RNA Viruses Using Cas13

Graphical Abstract

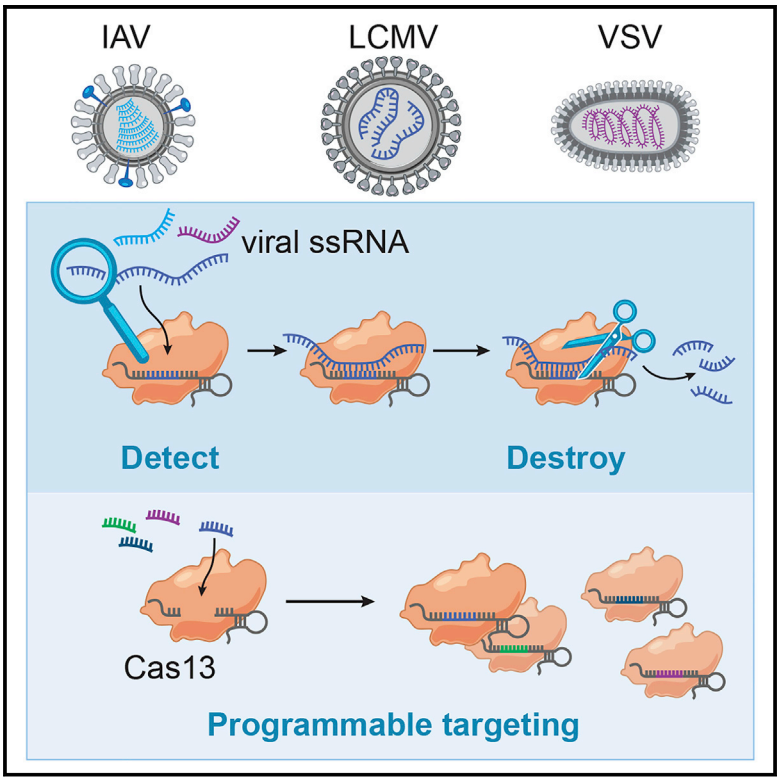

Authors

Catherine A. Freije, Cameron Myhrvold, Chloe K. Boehm, ..., Nathan L. Yozwiak, Feng Zhang, Pardis C. Sabeti

Correspondence

cfreije@broadinstitute.org (C.A.F.), cmyhrvol@broadinstitute.org (C.M.), pardis@broadinstitute.org (P.C.S.)

In Brief

Freije et al. demonstrate that Cas13 can be programmed to target and destroy the genomes of diverse mammalian single-stranded RNA viruses. They identify design principles for efficient Cas13 targeting of viral RNA and create companion Cas13-based diagnostics to rapidly measure the effects of Cas13 targeting.

Highlights

- Thousands of potential Cas13 target sites are present in ssRNA viral genomes
- Cas13 is a potent antiviral against three diverse ssRNA viruses in cell culture
- Optimal Cas13 target sites and design criteria are identified via genome-wide screen
- Companion Cas13-based diagnostics can be used to assess the effects of targeting

Freije et al., 2019, Molecular Cell *76*, 826–837
December 5, 2019
https://doi.org/10.1016/j.molcel.2019.09.013

CellPress

CellPress

Molecular Cell
Resource

Programmable Inhibition and Detection of RNA Viruses Using Cas13

Catherine A. Freije,[1,2,12,*] Cameron Myhrvold,[1,3,12,13,*] Chloe K. Boehm,[1] Aaron E. Lin,[1,2] Nicole L. Welch,[1,2] Amber Carter,[1] Hayden C. Metsky,[1,4] Cynthia Y. Luo,[1,3] Omar O. Abudayyeh,[1,5,6,7,8] Jonathan S. Gootenberg,[1,5,6,7,9] Nathan L. Yozwiak,[1,3] Feng Zhang,[1,5,6,7,10] and Pardis C. Sabeti[1,2,3,10,11,*]

[1]Broad Institute of Massachusetts Institute of Technology (MIT) and Harvard, Cambridge, MA 02142, USA
[2]PhD Program in Virology, Division of Medical Sciences, Harvard Medical School, Boston, MA 02115, USA
[3]Department of Organismic and Evolutionary Biology, Harvard University, Cambridge, MA 02138, USA
[4]Department of Electrical Engineering and Computer Science, MIT, Cambridge, MA 02142, USA
[5]McGovern Institute for Brain Research, MIT, Cambridge, MA 02139, USA
[6]Department of Brain and Cognitive Science, MIT, Cambridge, MA 02139, USA
[7]Department of Biological Engineering, MIT, Cambridge, MA 02139, USA
[8]Department of Health Sciences and Technology, MIT, Cambridge, MA 02139, USA
[9]Department of Systems Biology, Harvard Medical School, Boston, MA 02115, USA
[10]Howard Hughes Medical Institute (HHMI), Chevy Chase, MD 20815, USA
[11]Department of Immunology and Infectious Disease, T.H. Chan Harvard School of Public Health, Boston, MA 02115, USA
[12]These authors contributed equally
[13]Lead Contact
*Correspondence: cfreije@broadinstitute.org (C.A.F.), cmyhrvol@broadinstitute.org (C.M.), pardis@broadinstitute.org (P.C.S.)
https://doi.org/10.1016/j.molcel.2019.09.013

SUMMARY

The CRISPR effector Cas13 could be an effective antiviral for single-stranded RNA (ssRNA) viruses because it programmably cleaves RNAs complementary to its CRISPR RNA (crRNA). Here, we computationally identify thousands of potential Cas13 crRNA target sites in hundreds of ssRNA viral species that can potentially infect humans. We experimentally demonstrate Cas13's potent activity against three distinct ssRNA viruses: lymphocytic choriomeningitis virus (LCMV); influenza A virus (IAV); and vesicular stomatitis virus (VSV). Combining this antiviral activity with Cas13-based diagnostics, we develop Cas13-assisted restriction of viral expression and readout (CARVER), an end-to-end platform that uses Cas13 to detect and destroy viral RNA. We further screen hundreds of crRNAs along the LCMV genome to evaluate how conservation and target RNA nucleotide content influence Cas13's antiviral activity. Our results demonstrate that Cas13 can be harnessed to target a wide range of ssRNA viruses and CARVER's potential broad utility for rapid diagnostic and antiviral drug development.

INTRODUCTION

CRISPR-Cas systems have revolutionized our ability to edit genes and modulate gene expression; however, these systems evolved in nature to defend bacteria against invading bacteriophages and other foreign nucleic acids (Wright et al., 2016). DNA-targeting effectors like Cas9 provide protection against invading DNA bacteriophages, and type III and VI effectors with RNA-targeting activity enable defense against RNA pathogens. This suggests that CRISPR effectors could be repurposed to aid in defending mammalian cells against both DNA and RNA viruses. Indeed, recent applications of Cas9 have demonstrated that CRISPR effectors can inhibit replication of double-stranded DNA viruses or single-stranded RNA (ssRNA) viruses with DNA intermediates in mammalian cells (Liu et al., 2015; Ophinni et al., 2018; Price et al., 2015; Ramanan et al., 2015; Roehm et al., 2016; Wang et al., 2018; Yin et al., 2017). However, about two-thirds of viruses that can infect humans have ssRNA genomes, and only 2.5% of those viruses have DNA intermediates that could be targeted with Cas9 (Brister et al., 2015; Woolhouse and Adair, 2013; Woolhouse et al., 2016). Furthermore, many ssRNA viruses cause human disease and lack US Food and Drug Administration (FDA)-approved therapies (De Clercq and Li, 2016), underscoring the need for additional antiviral strategies. Recently characterized RNA- and DNA-targeting orthologs of Cas9 are less likely to be able to address this need, as they have low RNA-cleavage efficiency and could induce off-target effects on cellular DNA (Price et al., 2015; Strutt et al., 2018).

RNA-targeting CRISPR effectors could offer a promising alternative antiviral approach. Recent studies of the class 2 type VI CRISPR effector Cas13 have highlighted its ability to efficiently target and cleave RNA in several model systems, including mammalian cells (Abudayyeh et al., 2016, 2017; Aman et al., 2018a, 2018b; Bawage et al., 2018; Cox et al., 2017; Zhao et al., 2018; Konermann et al., 2018). Furthermore, Cas13 is able to process its CRISPR array and release individual CRISPR RNA (crRNAs) (Shmakov et al., 2015), allowing for multiplexed targeting applications. In addition to CRISPR array processing activity, Cas13 has collateral cleavage activity that has been harnessed for diagnostic applications, such as specific high-

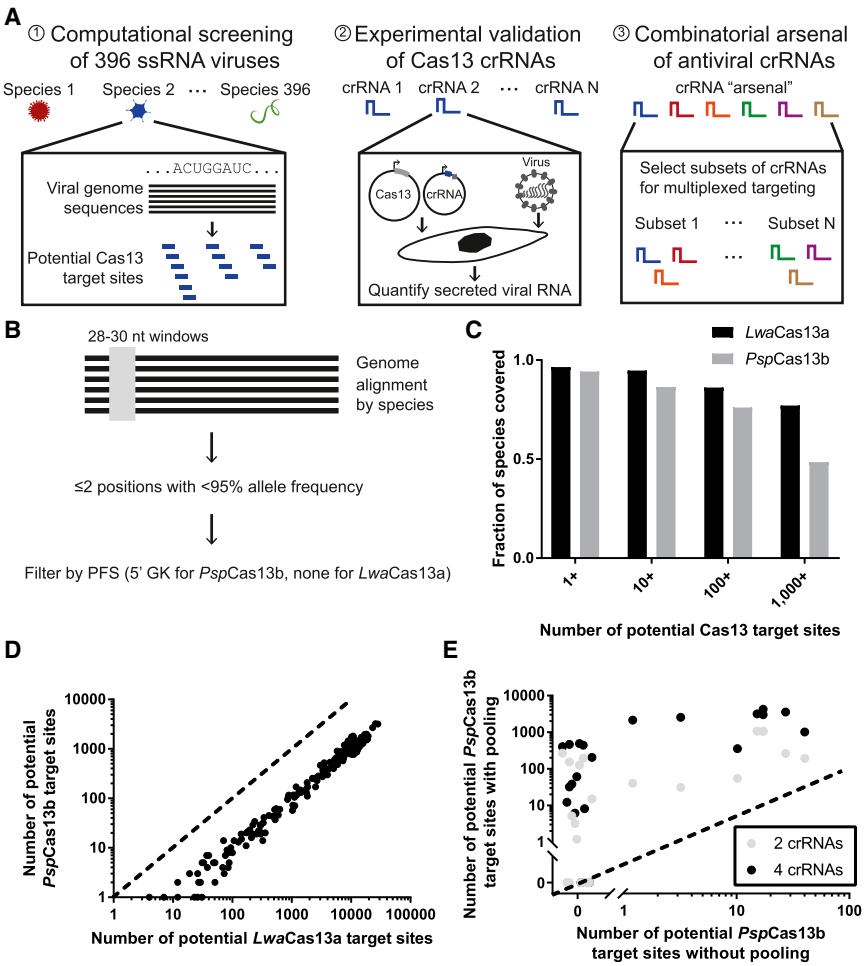

Figure 1. Potential Cas13 Target Sites Are Abundant in Viral Genomes

(A) Overview of the strategy for identifying potent Cas13 target sites, which integrates computational screening and experimental validation to yield a combinatorial arsenal of crRNAs.

(B) Schematic of the approach for identifying conserved sites for Cas13 targeting.

(C) Fraction of human-associated ssRNA virome with at least 1, 10, 100, or 1,000 Cas13 target sites, based on known sequence diversity.

(D) Comparison of the number of *Lwa*Cas13a and *Psp*Cas13b target sites in the genomes of 396 human-associated ssRNA viruses.

(E) Effect of pooling 2 (gray) or 4 (black) crRNAs on the number of *Psp*Cas13b target sites identified by ADAPT for those viral species (n = 23) without targets as defined in (B).

In (D) and (E), each point is a viral species; dashed lines indicate x = y.

sensitivity enzymatic reporter unlocking (SHERLOCK) (Gootenberg et al., 2017, 2018; Myhrvold et al., 2018). However, many Cas13 orthologs have minimal off-target effects on the host transcriptome in mammalian cells, as determined in several recent studies (Abudayyeh et al., 2017; Bawage et al., 2018; Cox et al., 2017; Konermann et al., 2018). This suggests that Cas13 has potential as an antiviral platform if it can be programmed to efficiently target and destroy a wide variety of mammalian viruses. Establishing such a Cas13-based antiviral platform will require investigating the prevalence of target sites in ssRNA viral genomes, experimentally validating Cas13's antiviral activity when directed to these target sites, and uncovering strategies to optimize this activity (Figure 1A).

A programmable antiviral technology would allow for the rapid development of antivirals that can target existing or newly identified pathogens. In the past 50 years, 90 clinically approved antiviral drugs have been produced, but these antivirals only treat nine viral diseases, only four of which are ssRNA viruses. Vaccines have emerged as the predominant approach to combating viral diseases, but only 16 viruses have FDA-approved vaccines (De Clercq and Li, 2016). Many new efforts have emerged to develop antiviral drugs, such as small-molecule screening approaches focused on identifying inhibitors of viral and host targets. Identifying potent inhibitors of these targets often requires biological or mechanistic understanding, which could slow antiviral development in the face of drug resistance or emerging pathogens. Furthermore, human viral pathogens are quite diverse and evolve rapidly, underscoring both the challenge of developing and great need for adaptable antiviral therapeutic platforms.

Here, we harness Cas13's programmable RNA-targeting activity to develop an end-to-end technology platform called Cas13-assisted restriction of viral expression and readout (CARVER) that combines Cas13-mediated cleavage of viral RNA with a rapid, Cas13-based diagnostic readout using the SHERLOCK platform (Gootenberg et al., 2017). We first explored the broad utility of Cas13 for targeting mammalian ssRNA viruses by computationally analyzing >350 viral genomes from species known or predicted to infect humans. We then experimentally tested Cas13's ability to inhibit viral replication in three distinct ssRNA viruses: lymphocytic choriomeningitis virus (LCMV); influenza A virus (IAV); and vesicular stomatitis virus (VSV). To define crRNA design criteria, we performed a genome-wide LCMV screen. We further optimized this antiviral approach by investigating the importance of Cas13 localization and multiplexing crRNAs and compared the performance of Cas13 and short hairpin RNAs (shRNAs). Finally, we explored whether Cas13 targeting would result in mutations at the site of crRNA targeting. Together, these investigations establish CARVER as a powerful antiviral and diagnostic technology platform for a wide variety of ssRNA viruses.

RESULTS

Computational Analysis Identifies Cas13 Sites in >350 Human-Associated Viral Genomes

To evaluate the future prospects of Cas13 as a comprehensive antiviral strategy, we explored the abundance of Cas13 target

sites in the genomes of human-associated viruses (HAVs). HAVs are defined as viral species that can infect humans or with close relatives that infect humans. There are 396 ssRNA viral species annotated as human associated in the NCBI genome neighbors database (Brister et al., 2015; Woolhouse and Adair, 2013; Woolhouse et al., 2016), at least 20 of which are high-risk human pathogens (Table S1). We began by generating an alignment for each genome segment of each of the 396 species (see STAR Methods for details). Given the extreme diversity of ssRNA viruses, a key challenge is to identify enough sites for Cas13 targeting within these alignments to cover the total diversity for a given species and to be deemed functional following experimental validation.

We started with a computational analysis of viral genome sequences to identify highly conserved potential target sites for Cas13, followed by experimental validation in cell culture models, to yield an arsenal of antiviral crRNAs that can be multiplexed in a combinatorial fashion (Figure 1A). For computational screening and experimental validation, we used Cas13a from *Leptotrichia wadei* (*Lwa*Cas13a) and Cas13b from *Prevotella sp. P5-125* (*Psp*Cas13b). Both of these Cas13 orthologs efficiently knockdown mRNA in mammalian cells but could have varying optimal target sites due to differences in cleavage activity and protospacer flanking site (PFS) requirements (Abudayyeh et al., 2017; Cox et al., 2017).

To identify potential Cas13 target sites, we aligned viral genomes and defined a potential target site as a 28- or 30-nt window where most or all positions are conserved, allowing only 2 or fewer positions to have an allele frequency <95% (Figure 1B). We filtered potential target sites to ensure the presence of the PFS specific to each Cas13 ortholog (Abudayyeh et al., 2017; Cox et al., 2017). We determined that 94.6% of the 396 ssRNA HAVs have $\geq$10 putative Cas13a target sites and 86.3% have $\geq$10 putative Cas13b target sites, based on known sequence diversity (Figure 1C; Table S2). Due to Cas13b's PFS requirements, Cas13b has fewer potential target sites than Cas13a. However, potential Cas13 target sites are quite numerous overall: 86% of ssRNA HAVs have $\geq$100 Cas13a target sites and 76% have $\geq$100 Cas13b target sites (Figures 1C and 1D). Furthermore, the number of potential Cas13b target sites that can cover >95% of available genome sequences, as measured by ADAPT (H.C.M. and P.C.S, unpublished data), can be enhanced by pooling up to four crRNAs; this allows sites with higher sequence diversity to be targeted (Figure 1E; see STAR Methods for details). These results underscore that Cas13 can potentially be applied to target a wide range of mammalian ssRNA viruses.

Cas13 Has Potent Antiviral Activity against Multiple ssRNA Viruses in Cell Culture

To evaluate Cas13's potential to serve as a programmable antiviral platform for targeting ssRNA viruses, we measured Cas13's antiviral effects against three ssRNA viruses with distinct sequence diversity and replication strategies. We hypothesized that Cas13 crRNAs, when directed to cleave viral RNA, would potently inhibit viral replication (Figure 2A) and subsequently tested whether expression of Cas13 and virus-specific crRNAs in cell culture would reduce viral RNA following infection with LCMV, IAV, or VSV (Figure 2B).

We initially tested the antiviral activity of *Lwa*Cas13a against the model mammarenavirus LCMV. Mammarenaviruses, within family *Arenaviridae*, are enveloped viruses with a bi-segmented (large: L, ~7.3 kb; small: S, ~3.5 kb), ambisense ssRNA genome with the life cycle, RNA genome, and RNA replication intermediates restricted to the cytoplasm of infected cells. Several mammarenaviruses cause hemorrhagic fever disease in humans (e.g., Lassa fever virus) and pose important public health problems in their endemic regions. These viruses lack virus-specific, FDA-approved vaccines or therapeutics (Geisbert, 2018), making them a prime candidate for development of new antiviral approaches. We designed 11 pilot crRNAs (pL1–pL6 and pS1–pS5), with spacers 28 nt in length (Abudayyeh et al., 2016), to target various locations along the L and S segments.

*Lwa*Cas13a efficiently reduced LCMV viral RNA (vRNA) levels for a majority of pilot crRNAs tested, even at high MOI. We tested the pilot crRNAs against LCMV at a high MOI (MOI = 5) in HEK293FT cells and observed a 2- to 14-fold reduction in viral RNA with five of six L-segment-targeting crRNAs (83.33%) as measured by RT-qPCR 48 h post infection (hpi) (Figure 2C). L-targeting and S-targeting crRNAs mediated a reduction in LCMV viral RNA when transfection of *Lwa*Cas13a and these crRNAs was performed prior to or post-LCMV infection at high MOI (MOI = 5; Figures 2C, S1A, and S1B). *Lwa*Cas13a's antiviral activity, when Cas13 is expressed prior to infection, persisted at low MOIs (Figure S1C), and *Lwa*Cas13a's catalytic activity and cytoplasmic localization were required for antiviral activity against LCMV (Figure S1D). Furthermore, *Lwa*Cas13a targeting in the context of LCMV infection did not lead to changes in cell viability (Figure S1E).

We then designed a set of crRNAs to target another high priority virus, IAV, which has a different replication strategy and cellular localization than LCMV. IAV is a negative sense ssRNA virus with eight genomic segments of varying length (ranging from 0.89 to 2.3 kb), and IAV's viral RNA and complementary viral RNA remain in the nucleus although the mRNAs reside in the cytoplasm. We designed five IAV-targeting crRNAs to target both the mRNA and the complementary viral RNA. We tested *Psp*Cas13b's antiviral activity against IAV in Madin-Darby canine kidney (MDCK) epithelial cells by electroporating plasmids expressing individual crRNAs and *Psp*Cas13b and measuring IAV viral RNA levels in the cell culture supernatant by RT-qPCR (Figure 2B). *Psp*Cas13b reduced IAV viral RNA levels by 7- to 22-fold 24 hpi (Figure 2D).

To further demonstrate the generalizability of Cas13 targeting, we evaluated whether *Psp*Cas13b could inhibit the neurotropic RNA virus VSV, which has a negative sense ssRNA genome (~11 kb) composed of a single linear segment. VSV is a prototype for studies of nonsegmented, negative-strand ssRNA viruses, making it a great candidate for measuring Cas13's antiviral activity against this class of RNA viruses that make up 37.8% of the human-associated RNA virome. We designed crRNAs against conserved regions of the two main VSV serotypes, Indiana and New Jersey, and selected two target sites for each gene. HEK293FT cells expressing *Psp*Cas13b and VSV-specific crRNAs had between 7.8- and 43.3-fold decreased levels of secreted VSV viral RNA 48 hpi (MOI = 1; Figures 2B and 2E). Together, our results demonstrate that both *Lwa*Cas13a

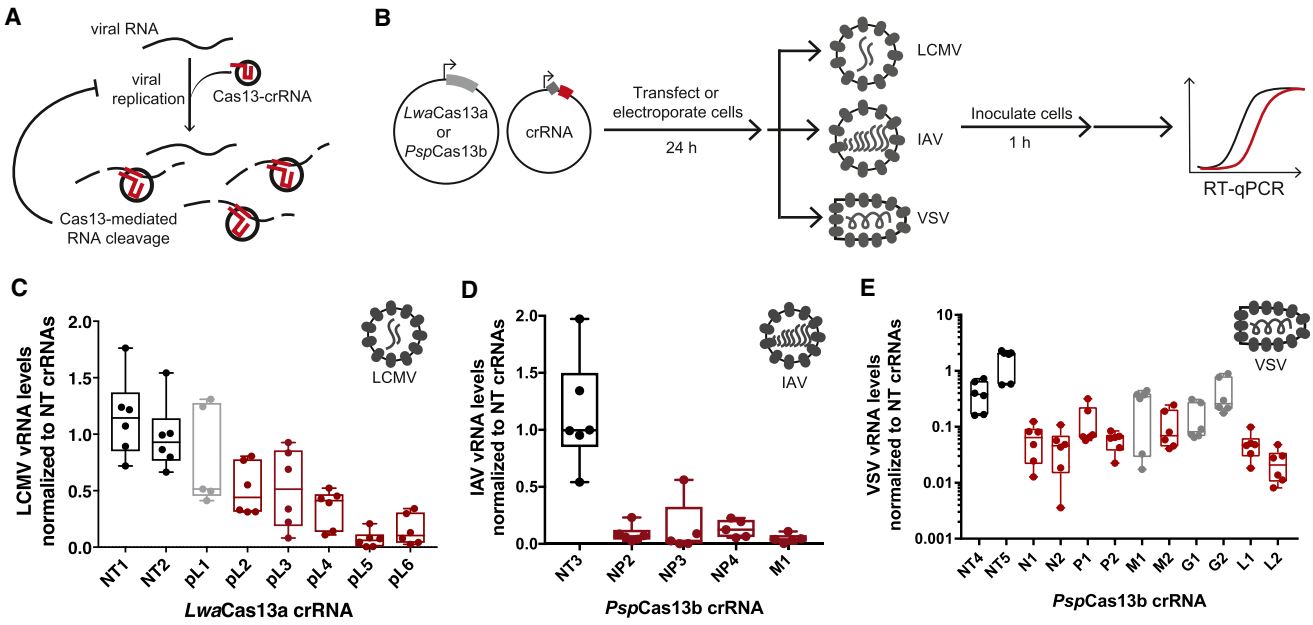

Figure 2. Cas13 Efficiently Reduces Levels of Viral RNA in Mammalian Cells

(A) Schematic illustrating Cas13 targeting and cleavage of viral RNA (vRNA) to inhibit viral replication.

(B) Experimental setup for assays evaluating the targeting activity of *Lwa*Cas13a and *Psp*Cas13b against multiple ssRNA viruses. Red boxes, spacers; gray diamonds, direct repeats.

(C) Normalized LCMV vRNA levels 48 hpi when transfection of *Lwa*Cas13a and pilot L-targeting or non-targeting control crRNA plasmids is performed 24 h prior to infection (MOI = 5).

(D) Normalized IAV vRNA levels 24 hpi when transfection of *Psp*Cas13b and pilot NP-targeting, M-targeting, or non-targeting control crRNA plasmids is performed 24 h prior to infection (MOI = 0.01).

(E) Normalized VSV vRNA levels 48 hpi when transfection of *Psp*Cas13b and pilot VSV-targeting crRNA plasmids is performed 24 h prior to infection (MOI = 1). In (C)–(E), individual points are biological replicates; n = 5–6. Red, $p \leq 0.01$ compared to all non-targeting crRNAs using a Student's t test. L, LCMV L segment; NT, non-targeting; p, pilot. See STAR Methods for normalization details.

and *Psp*Cas13b can efficiently and specifically cleave viral RNA in 3 distinct ssRNA viruses, highlighting Cas13's future potential as a potent inhibitor of viral RNA for a wide variety of human ssRNA pathogens.

A Genome-wide Screen against LCMV Reveals Viral RNA Targeting Principles for Cas13

To increase our understanding of the design criteria for Cas13 targeting of viral RNAs, we designed a set of crRNAs tiling the entire LCMV genome. These covered the L and S genome segments (vRNA), both antigenomic segments (viral complementary RNA [vcRNA]), as well as the corresponding mRNAs, resulting in 283 crRNAs that target both negative-sense and positive-sense RNAs (Figures 3A and S2A). We transfected HEK293FT cells with a construct expressing cytoplasmic-localized *Lwa*Cas13a fused to blue fluorescent protein (BFP), followed by infection (MOI = 1) with recombinant LCMV expressing GFP (Ngo et al., 2015). We monitored GFP expression post-infection, which strongly correlated with viral RNA levels (Figures S2B–S2F). We defined active crRNA target sites as regions where *Lwa*Cas13a significantly reduced GFP levels (false discovery rate [FDR] $\leq$ 0.05) with $\geq$2-fold reduction in GFP fluorescence as compared to non-targeting crRNA controls (Figure S3A).

The genome-wide screen identified 124 active crRNA target sites (44% of tested sites; Figure 3B), many of which have high-nucleotide sequence conservation. Although nearly all anti-coding-sense sites were active (92%), the coding sense (31%) had far fewer active sites (Figure S3B). Active coding-sense sites clustered into targeting "hotspots" along the viral genome, which were closer than expected by chance ($p < 10^{-4}$; Figures S3C and S3D), prompting us to evaluate the sequence conservation in these regions. The S segment, which has higher levels of nucleotide conservation across all strains of LCMV compared to the L segment ($p < 10^{-15}$; Figure S3E; see STAR Methods for details), had a higher frequency of active sites (43% of all S target sites versus 18% of all L target sites). A high proportion of active coding-sense sites were conserved (78.6%), and 30% of tested conserved sites were active compared to 24% of non-conserved sites (Figure 3C). These results suggest that selecting conserved regions for experimental validation of Cas13 antiviral activity could increase the probability of identifying active sites, consistent with previous observations for other nucleic-acid-based approaches (von Eije et al., 2008).

We hypothesized that *Psp*Cas13b would similarly have increased knockdown efficiency if directed toward conserved regions of the LCMV genome. To test this, we designed 23 crRNAs targeting the L gene vRNA in regions with high- or low-nucleotide-level sequence conservation. Indeed, when crRNAs targeted highly conserved regions, a higher proportion were active target sites compared to poorly conserved regions

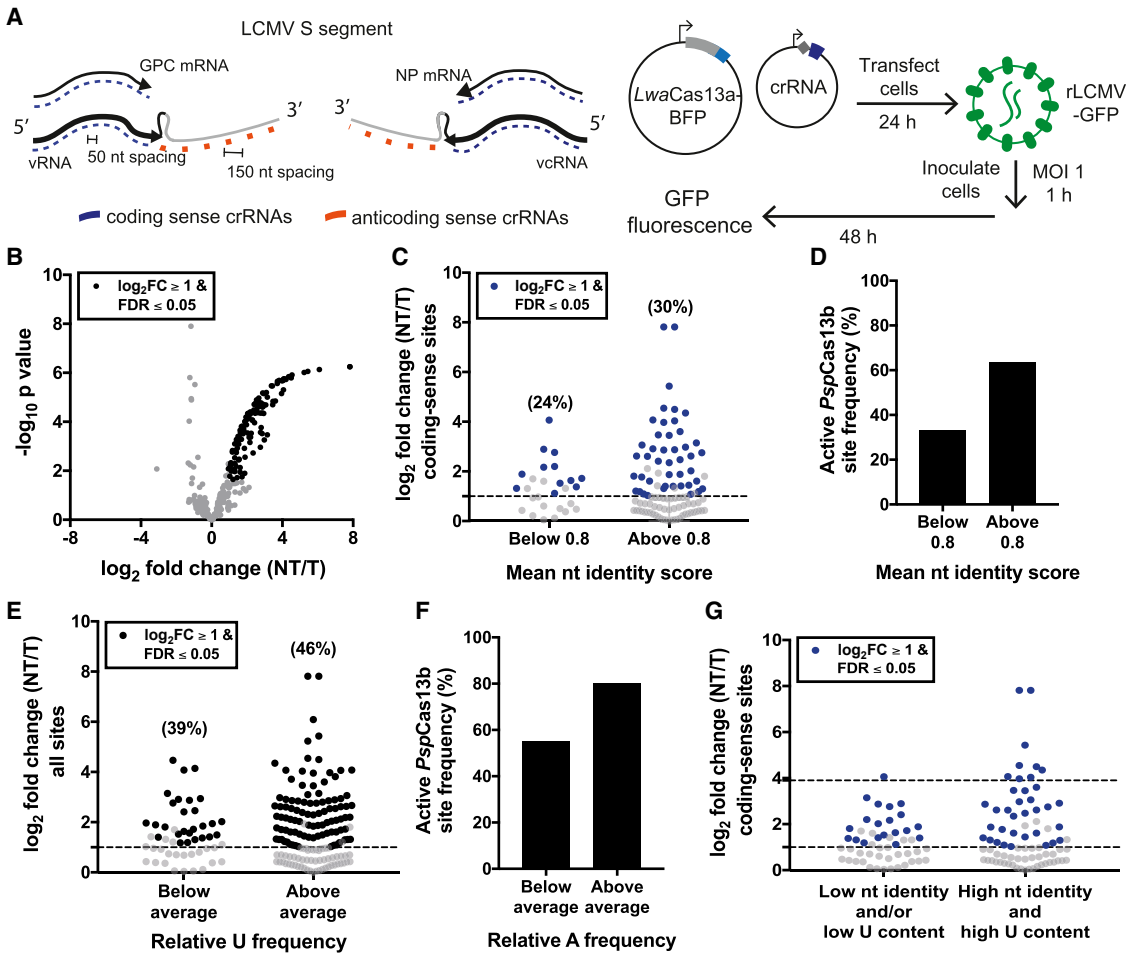

Figure 3. Identification of Cas13 Target Sites and crRNA Design Criteria

(A) Schematic of LCMV full-genome screen using *Lwa*Cas13a, crRNA design, and experimental setup. Tiled crRNAs were designed to target the coding (50-nt spacing) and anticoding sense (150-nt spacing) strands of both segments of LCMV. Cas13 activity was assessed by measuring GFP expression 48 hpi with a recombinant LCMV expression GFP (rLCMV-GFP) with inoculation occurring post *Lwa*Cas13a and crRNA plasmid transfection.

(B) Volcano plot of the results of the LCMV genome screen. Each point represents a single tiled crRNA. To calculate fold changes, each tiled crRNA was compared to all non-targeting controls. Tiled crRNAs with $\log_2FC \geq 2$ and FDR ≤ 0.05, black.

(C) Log_2FC of all coding-sense targeting tiled *Lwa*Cas13 crRNAs binned by whether the mean nt identity score is above or below 0.8 (see STAR Methods for details). Tiled coding-sense targeting crRNAs with $\log_2FC \geq 2$ and FDR ≤ 0.05, blue.

(D) Frequency as a percentage of *Psp*Cas13b crRNAs tested that were active binned by mean nt identity score above or below 0.8.

(E) Log_2FC of all targeting tiled *Lwa*Cas13 crRNAs binned by whether the relative U frequency flanking the target site is above or below the average U frequency of gene's target site (see STAR Methods for details). Tiled targeting crRNAs with $\log_2FC \geq 2$ and FDR ≤ 0.05, black.

(F) Percentage of *Psp*Cas13b crRNAs tested that were active binned by relative A frequency of the gene's target site.

(G) Log_2FC of all coding-sense targeting tiled *Lwa*Cas13 crRNAs binned by whether both the mean nt identity score and relative U frequency are high or not. Tiled coding-sense targeting crRNAs with $\log_2FC \geq 2$ and FDR ≤ 0.05, blue.

In (B), (C), (E), and (G), all tiled crRNAs had n = 3; p value was calculated using a Student's t test, and FDR was corrected using the Benjamini-Hochberg method. For (D) and (F), *Psp*Cas13b crRNA n = 9. *Psp*Cas13b active sites had measured viral RNA fold change of ≥ 1.5, and $p \leq 0.05$ compared to all non-targeting crRNAs using a Student's t test.

(63.6% versus 33.3%; Figure 3D). Further, crRNAs designed against regions conserved among all strains of LCMV were more likely to be active than those targeting conserved regions specific to the LCMV strain being tested (88.8% versus 43.75%; Figure S3F).

Further analysis of the genome tiling results showed that target RNA nucleotide content, but not experimentally derived RNA secondary structure, influences crRNA activity. Targeting efficiency of overlapping crRNAs, designed against either the coding or anticoding sense, was anticorrelated, showing preferential activity for one of the senses (Figure S3G). We hypothesized that this anticorrelation could be related to the frequency of Us flanking target sites given that *Lwa*Cas13a cleaves at Us outside the crRNA binding site (Abudayyeh et al., 2016; Gootenberg et al., 2018). In concordance with this hypothesis, a greater percentage of target sites near regions with above-average gene-level

U frequency were active compared to sites near regions with below-average U frequency (46% versus 39%; Figure 3E). *Psp*Cas13b, in contrast, cleaves at As (Gootenberg et al., 2018), and we observed that a greater percentage of sites near regions with above-average gene-level A frequency were active target sites compared to those with below-average A frequency (80% versus 55%; Figure 3F). Together, these results suggest that nucleotide context near the target site, specifically the presence of cleavage nucleotides, influences the likelihood a crRNA will be active and is an important consideration due to the biased nucleotide composition of viral genomes (van Hemert et al., 2016). When considering both conservation and target RNA nucleotide content, we found that nine of ten of sites with >15-fold knockdown possessed both high levels of nucleotide conservation and high U content neighboring the crRNA target site (Figure 3G).

We hypothesized that RNA accessibility would also influence which regions of the LCMV vRNA, vcRNA, and viral mRNAs had effective viral knockdown. To examine this relationship, we used SHAPE-MaP (Siegfried et al., 2014) to characterize the RNA secondary structure of *in vitro* transcribed vRNA, vcRNA, and nucleoprotein (NP)-mRNA of the LCMV S segment. SHAPE-MaP reactivity scores were reproducible across replicates and confirmed the presence of secondary structure of LCMV's intergenic region (IGR) and the 5′ and 3′ ends of the genome (Perez and de la Torre, 2003; Salvato and Shimomaye, 1989; Figures S3H and S3I). However, comparing the reactivity scores of non-active target sites and active target sites, we did not observe a relationship within this dataset (Figure S3J).

Delivery of Cas13 ribonucleoprotein complexes (RNPs) offers an alternative approach to plasmid expression with faster kinetics, which could be useful in specific therapeutic contexts. As has been demonstrated with Cas13, Cas12, and Cas9, there are multiple expression modalities for Cas13 differing in expression kinetics and required dosages, which include plasmids, mRNAs, and RNPs (Bawage et al., 2018; Kim et al., 2014; Strecker et al., 2019; Zhao et al., 2018). Although alternative nucleic-acid-based therapeutics, like RNAi, would only require delivery of nucleic acid, these approaches have limitations largely due to off-target effects and limited on-target activity (Abudayyeh et al., 2017; Cox et al., 2017). We explored the RNA targeting efficiency of *Lwa*Cas13a and Cas13b from *Prevotella* sp. MA2016 (*Psm*Cas13b) RNPs against both luciferase and a selection of LCMV-directed crRNAs (Figures S4A and S4B). Both *Lwa*Cas13a and *Psm*Cas13b RNPs, transfected 4 h prior to infection, reduced viral RNA levels, demonstrating that multiple expression modalities can be used for Cas13-based viral RNA targeting applications (Figures S4C and S4D).

Optimizing Cas13 Targeting Using Multiplexing

The promise of Cas13 as a new platform for antiviral therapy would require its activity to be competitive with current gold standards of nucleic-acid-based therapeutics. To test this, we compared the performance of Cas13 crRNAs side by side with location-matched shRNAs. We found that *Psp*Cas13b-mediated inhibition of LCMV was comparable to that of shRNAs; tested crRNAs reduced viral RNAs between 4- and 10-fold compared to non-targeting crRNAs as measured by RT-qPCR (Figure 4A).

Delivery of multiple crRNAs or CRISPR arrays can be used to further enhance Cas13's antiviral effect. To measure the effect of multiplexing, we collected virus-containing supernatant 24 hpi and measured bulk levels of LCMV using the rapid viral inactivation method, HUDSON (heating unpurified diagnostic samples to obliterate nucleases) and Cas13-based detection platform, SHERLOCK (Gootenberg et al., 2017; Myhrvold et al., 2018; Figure 4B). Pooling multiple validated *Lwa*Cas13a crRNAs successfully reduced viral replication, with higher amounts of pooling enhancing this effect (Figure 4C). Furthermore, because Cas13 is able to process its CRISPR array and release individual crRNAs (Shmakov et al., 2015), we showed that *Psp*Cas13b transfected with a CRISPR array can deliver up to four crRNAs simultaneously for viral RNA targeting (Figure 4D). Multiplexing is therefore an inherent and powerful advantage of Cas13-based therapies.

Development and Testing of CARVER as an End-to-End Platform for Detecting and Destroying Viral RNA

Unlike other nucleic-acid-based approaches and quite remarkably, Cas13 can be applied in both viral detection and knockdown contexts, creating a potential for an end-to-end platform for diagnosis and treatment of infectious diseases. Although we can measure the response to Cas13-crRNA expression using recombinant GFP-expressing LCMV in cell culture, rapid measurement of wild-type viral RNA levels would be required in clinical settings. To address this, we developed CARVER as a platform for measuring viral RNA levels following Cas13 targeting in real time using the Cas13-based nucleic acid detection technology SHERLOCK (Gootenberg et al., 2017, 2018; Myhrvold et al., 2018; Figure 4E). SHERLOCK uses isothermal amplification with recombinase polymerase amplification (RPA) followed by *in vitro* transcription and Cas13 detection with a cleavage reporter. We paired Cas13-based targeting with a SHERLOCK assay that measured LCMV RNA levels in cell culture supernatant following Cas13 treatment. We isolated LCMV RNA in the supernatant using HUDSON, which rapidly inactivates the nucleases present in complex samples with a combination of heat and chemical treatment, and used SHERLOCK for RNA detection (Myhrvold et al., 2018; Figures S5A and S5B). To highlight the utility of CARVER, we targeted LCMV with a selection of crRNAs identified in the LCMV full-genome screen and rapidly detected LCMV levels; SHERLOCK fluorescence was reduced by >15-fold for 4 out of 5 of the crRNAs tested (Figure S5C).

Because Cas13's targeting activity is highly specific, tolerating only a few mismatches for activation, CARVER can also be used to detect single-nucleotide changes in the resultant viral populations. To achieve this, we developed a SHERLOCK assay that identified the F260L mutation associated with the switch from acute to persistent infection by LCMV (Sullivan et al., 2011; Figures 4F, S5D, and S5E). The turnaround time for both the bulk LCMV and F260L assays is <2 h, with limited equipment requirements, thereby providing rapid feedback about the effectiveness of treatment with Cas13 and information about specific viral mutations.

Additional Factors Mediating Cas13-based Targeting Effects against IAV

In order to explore additional strategies for enhancing Cas13's antiviral activity, we tested the effects of *Psp*Cas13b localization,

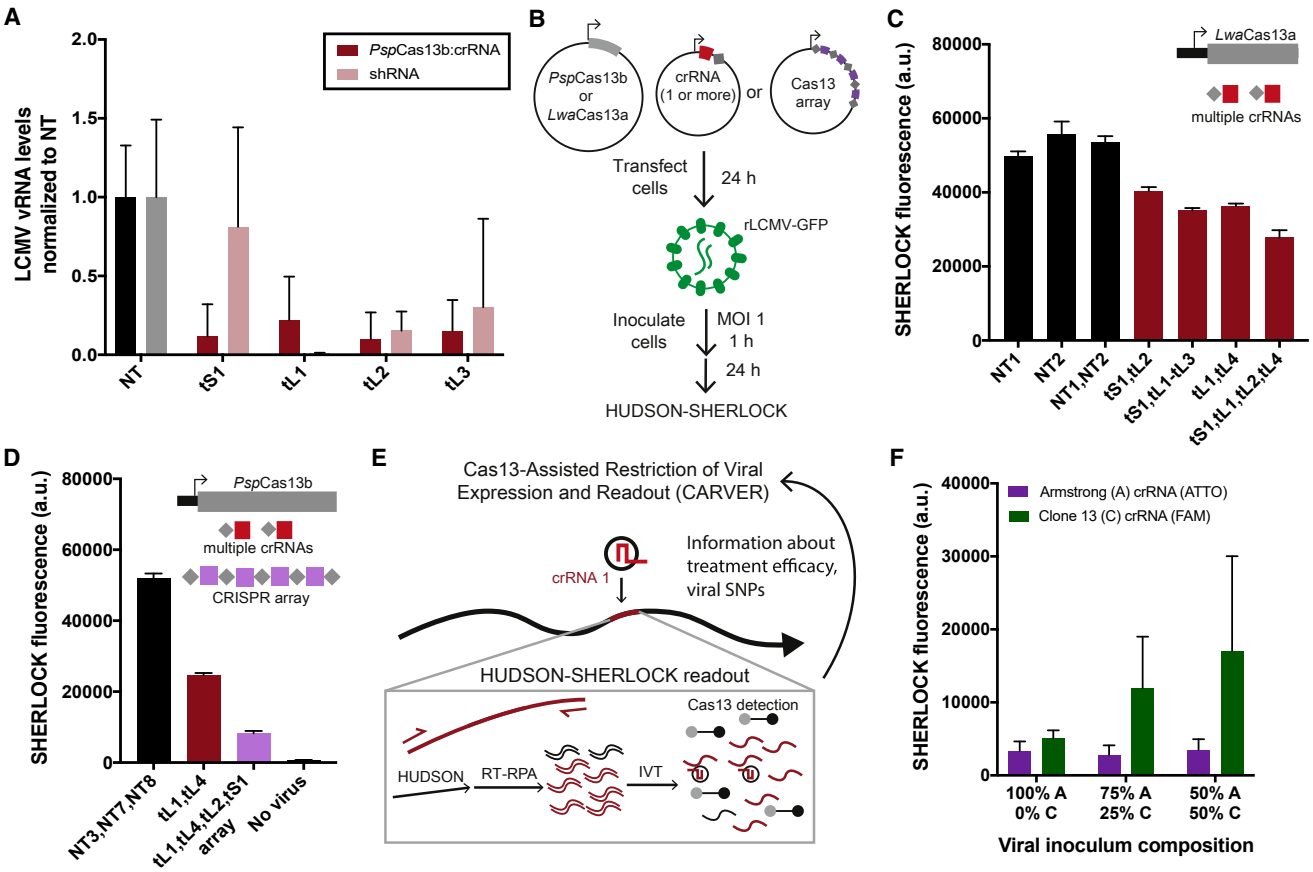

Figure 4. Enhanced Cas13-based Antivirals through Multiplexing and Paired Diagnostics

(A) Normalized vRNA levels comparing *Psp*Cas13b crRNAs to position-matched shRNAs. *Psp*Cas13b NT crRNA, NT3.

(B) Experimental setup for testing CARVER using LCMV.

(C) SHERLOCK fluorescence 24 hpi and 48 h post-transfection (hpt) of *Lwa*Cas13a and single or pooled crRNAs.

(D) SHERLOCK fluorescence with cells expressing *Psp*Cas13b and pooled crRNAs or CRISPR array.

(E) CARVER schematic of HUDSON-SHERLOCK readout paired with Cas13 viral RNA targeting.

(F) SHERLOCK fluorescence following a 1-h incubation using a two-color F260L SNP detection reaction combining *Lwa*Cas13a and *Psm*Cas13b, SNP-specific crRNAs and two cleavage reporters with fluorescein amidite (FAM) and ATTO fluorescence are shown (see STAR Methods for details). SHERLOCK fluorescence measured from cell culture supernatant following infection with mixed populations of LCMV Armstrong (A) and Clone 13 (C) strains is shown. Supernatant was collected 48 hpi.

For (A), (C), and (D), n = 3–5. S, LCMV S segment; t, tiled. Pooled or single targeting crRNAs, red; CRISPR arrays, purple; red boxes, spacers; gray diamonds, direct repeats. All time points were 24 hpi except (F), which is 48 hpi. For (A), (C), (D), and (F), error bars represent SD.

alternative cell types, and multiplexing approaches on this antiviral effect. We further investigated the IAV-targeting crRNAs (NP1–NP4 and M1) by electroporating *Psp*Cas13b and these crRNAs prior to infection and monitoring both viral RNA using RT-qPCR or IAV infectivity using median tissue culture infectious dose ($TCID_{50}$; Figure 5A). During the IAV viral life cycle, the RNA genome and cRNA genome reside in the nucleus of an infected cell and the viral mRNAs reside in the cytoplasm. We found that Cas13b localization to either the nucleus or the cytoplasm could impact crRNA activity, as crRNA NP1 only potently reduced IAV viral RNA levels when Cas13b was localized to the cytoplasm (i.e., targeting the mRNA) and there was no reduction in viral RNA when Cas13b was localized to the nucleus (i.e., targeting the complementary genomic RNA; Figure 5B). Cas13b antiviral activity was just as potent in adenocarcinomic human alveolar basal epithelial (A549) cells, reducing viral RNA by up to 20.6-fold (Figure 5C).

Because IAV is highly diverse and rapidly evolves, multiplexed approaches could be extremely beneficial for CARVER's ability to inhibit IAV replication. By pooling four crRNAs against NP, *Psp*Cas13b reduced IAV viral RNA by 8-fold, a modestly increased effect than induced by each individual NP-targeting crRNA alone (Figure 5D). Three of the four NP-targeting crRNAs we tested in the NP pool were already highly effective in MDCK cells (up to 8-fold knockdown of IAV viral RNA); thus we hypothesized whether this maximum observed effect is specific to measurement of IAV RNA levels following NP targeting and whether Cas13 cleavage of RNA could have even more drastic effects on resulting IAV infectivity. This could occur if partial genomic fragments were packaged and released into the cellular supernatant

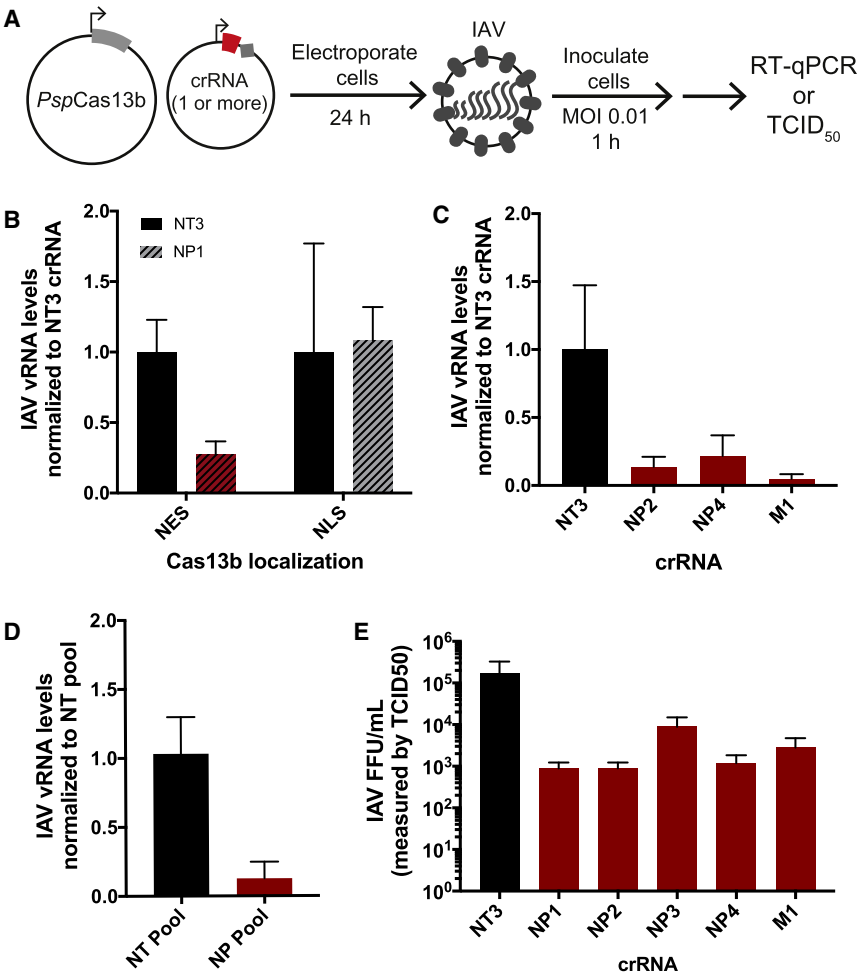

Figure 5. Additional Considerations for Improving Cas13-based Antivirals

(A) Experimental schematic of additional testing of *Psp*Cas13b's antiviral activity against IAV with plasmids introduced by electroporation and reduction of IAV post-infection measured by RT-qPCR or $TCID_{50}$.

(B) Normalized IAV vRNA 24 hpi with electroporation of NP-targeting or non-targeting crRNAs and nuclear export signal (NES)- or nuclear localization signal (NLS)-*Psp*Ca13b encoding plasmids in MDCK cells.

(C) Normalized IAV vRNA 24 hpi with electroporation of IAV-targeting or non-targeting crRNAs and NLS-*Psp*Ca13b encoding plasmids in A549 cells.

(D) Normalized IAV vRNA 24 hpi with electroporation of a pool of NP-targeting or of non-targeting crRNAs and NLS-*Psp*Ca13b encoding plasmids in MDCK cells.

(E) IAV focus-forming units/mL (FFU/mL) as measured $TCID_{50}$ 8 hpi with electroporation of IAV-targeting or non-targeting crRNAs and NES-*Psp*Ca13b encoding plasmids in MDCK cells.

For (B)–(D), n = 3; error bars, SD; red, $p \leq 0.01$ using Student's t test.

that would be detected by RT-qPCR measurements but would not produce infectious particles. Consistent with this hypothesis, we found that IAV infectivity was reduced by >300-fold for 2 of 5 crRNAs tested and >100-fold for 4 of 5 crRNAs tested 8 hpi (Figure 5E).

Mutations at the crRNA Target Site Are Not Detected in Viral Populations following Cas13 Treatment

The viral population secreted from cells following Cas13 treatment may have mutations within or near the crRNA binding site that could lead to crRNA resistance. To test for this possibility, we extracted viral RNA from the virus-containing supernatant of HEK293FT cells after 48 h of infection with LCMV (MOI = 1) for 5 LCMV-targeting crRNAs, 2 non-targeting controls, and mock transfected cells (no Cas13b; Figure 6A). We prepared duplicate unbiased, metagenomic sequencing libraries from each of these samples. Mean LCMV genome coverage of each library ranged from 847 to 5,414 (mean: 2,606) across both segments of the LCMV genome.

In our experiments, we did not detect mutations within the crRNA target site or see evidence of elevated mutation rates in the secreted LCMV viral populations. The consensus LCMV sequences across all sample populations were identical (Data S1), indicating that Cas13 targeting does not affect the majority population after 48 h of infection. We then investigated whether Cas13 targeting could lead to emergence of single-nucleotide minority variants (SNVs) that could cause crRNA resistance. We determined SNVs to be an allele present in both libraries, with an allele frequency >0.5%, and no strand bias (see STAR Methods for details). The number of detected SNVs and consequential mutation rate were similar between conditions with no Cas13, non-targeting crRNAs, and targeting crRNAs (Figure 6B; Table S3). Furthermore, no mutations were observed at the crRNA target sites in any of the conditions tested, despite high coverage (>400×) across all target sites and all conditions (Figure 6C).

DISCUSSION

Here, we showed that the CRISPR-Cas effector Cas13 can effectively target multiple distinct mammalian ssRNA viruses and highlighted CARVER's broader potential for diagnosis and treatment of ssRNA viruses. Our computational analysis uncovered numerous potential Cas13 target sites within >300 ssRNA HAV genomes, and subsequent experimental testing demonstrated that targeting conserved regions and sites with a high frequency of cleavage nucleotides influences Cas13's targeting activity against viral RNAs. Future testing of Cas13's antiviral activity against other viral species, including DNA viruses with RNA intermediates, could expand upon viral crRNA design principles. Such advances would aid in the full realization of CARVER as a platform that enables informed Cas13-based antiviral treatment strategies.

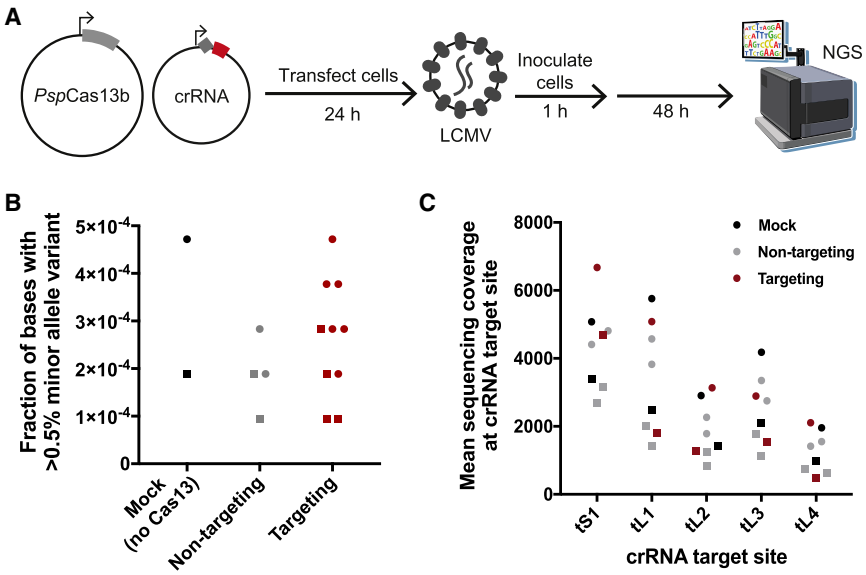

Figure 6. Analysis of Viral Mutations following Cas13 Treatment

(A) Schematic of the sequencing experiments where transfection is followed by LCMV infection (MOI = 1) and virus-containing supernatant is collected 48 hpi.

(B) Frequencies of bases with >0.5% minor allele variants normalized by genome length 48 hpi, as measured by next-generation sequencing (NGS) of virus-containing supernatants, for mock (black), non-targeting (gray), and targeting (red) conditions.

(C) Mean sequencing coverage at each of the crRNA target sites for mock (black), non-targeting (gray), and targeting crRNA at the given site (red). Mean was calculated from the coverage across both library constructions.

For (B) and (C), data from n = 2 independent experiments (circles and squares) are shown.

LCMV, IAV, and VSV are optimal test cases for CARVER, as clinically or scientifically impactful viruses in need of effective, alternative antiviral technologies. LCMV is a model viral system for studying mammarenaviruses, many of which cause hemorrhagic fever in humans, including Lassa fever virus. Lassa fever virus lacks a virus-specific, FDA-approved vaccine or antiviral and remains challenging to diagnose due to its high sequence diversity (Andersen et al., 2015; Geisbert, 2018; Raabe and Koehler, 2017). Approaches like CARVER offer a promising new solution to this unmet need. Similarly, IAV is a very diverse viral pathogen with high seasonal prevalence and pandemic potential. IAV's rapid evolution and propensity for recombination are obstacles for the development of both antivirals and vaccines and readily allow for the emergence of drug resistance. Lastly, we highlight Cas13's utility against an additional ssRNA virus, VSV, which could enable high-throughput studies of crRNA targeting properties because productive VSV infection results in cell death. Because recombinant forms of VSV can express alternative viral glycoproteins, successful testing of Cas13 would enable screening of glycoprotein-targeting crRNAs for numerous highly pathogenic RNA viruses that would otherwise require a biosafety level 4 facility. Despite different localization, sequence content, and replication biology, Cas13-based targeting potently inhibited all three ssRNA viruses tested.

Our results are striking in light of the challenges associated with targeting replicating viruses. Unlike previous applications of Cas13-based targeting of mRNA (Abudayyeh et al., 2017; Cox et al., 2017; Konermann et al., 2018; Zhao et al., 2018), viral RNA is actively replicating and evolving, and thus Cas13 must act at high enough efficiency to overcome this replication rate. Our LCMV cell culture experiments were performed at high MOI in cell lines that lack a functioning innate immune system, thus providing a stringent test of Cas13's ability to inhibit viral RNA (see Table S4). In contrast, infections in animal models occur at low MOIs as viral particles spread within tissues and a functional immune system is present. Measurements of viral infectivity following Cas13 targeting also indicated that Cas13 can have even stronger effects on viral infectivity. In an *in vivo* context, infectivity most accurately represents the amount of functional virus that can continue the infection.

Target site mutations can reduce the potency of many antiviral approaches, and thus, the propensity for these mutations to rise following treatment should be monitored. Previous studies of CRISPR-based antivirals using Cas9 reported mutations at target sites as early as 40 hpi (Wang et al., 2018) or within 3–7 days post infection (Liu et al., 2015; Ophinni et al., 2018; Roehm et al., 2016). However, we did not observe crRNA target site mutations following Cas13 treatment over the course of 48 h. This suggests (1) that Cas13 targeting does not lead to high mutation rates and (2) the resulting mutation rates are similar to those of small-molecule antivirals, where resistance does not emerge after a few rounds of viral replication (De Clercq and Li, 2016; Tang and Shafer, 2012). Future work will be required to evaluate the timescale and the degree to which viral RNAs can evolve resistance to Cas13 targeting.

These results highlight Cas13's potential for rapid antiviral design, as one does not need to test a large number of crRNA sequences to identify ones with potency. Previous studies have reported particular RNA structures are preferred cleavage sites for Cas13 (Abudayyeh et al., 2016) and target RNA structure has also been shown to impact other nucleic-acid-based antiviral approaches, like RNAi (Low et al., 2012; Westerhout et al., 2005). The lack of correlation between RNA accessibility and Cas13 activity in our data could be related to the presence of viral or host RNA binding proteins (e.g., LCMV nucleoprotein that coats the vRNA and vcRNA, but not the mRNAs) or a more complex relationship between secondary structure and sequence content. Therefore, *in vivo* determination of RNA structure would be necessary to fully understand its impact on Cas13 targeting and the optimal viral genomic regions to pursue.

As with many CRISPR-based technologies, *in vivo* delivery to cell types of interest remains a challenge. Indeed, our study suggests that, in the context of viral infection, delivery of Cas13 is especially important, as it sets a ceiling on the effect size that

can be observed. Although *in vivo* Cas9 demonstrations have become quite numerous (Wilson and Gilbert, 2018), Cas13 was discovered recently and is only beginning to be characterized and applied (Abudayyeh et al., 2016; East-Seletsky et al., 2016). Thus, *in vivo* applications for targeting mammalian RNA with Cas13 are in their infancy and will be demonstrated at scale in the coming years for programmable viral RNA targeting (Ma et al., 2019). Our study represents an essential first step in the repurposing of Cas13 for targeting mammalian viruses, setting the foundation for testing these applications *in vivo*.

Beyond potential antiviral applications, Cas13 targeting and viral knockdown can be used as a research tool to investigate viral replication, localization, and evolution. Specifically, previously developed catalytically dead mutants of Cas13 (dCas13) could be used to study viral RNA localization, and dCas13-fusion proteins with RNA-editing capabilities could be used to functionally characterize specific viral polymorphisms (Abudayyeh et al., 2017, 2019; Cox et al., 2017). Such tools will allow researchers to both visualize and perturb viral replication with a high degree of precision.

It is remarkable that the same protein, Cas13, has the potential to be used for both treatment and diagnosis of a broad range of viral diseases as part of an end-to-end platform. With CARVER, the CRISPR-Cas effector Cas13 can target multiple mammalian viruses as well as measure the effects of targeting and the viral response. Such technological flexibility is unprecedented for a single protein, and it underscores the power and promise of programmable nucleases, such as Cas13. Thus, Cas13 could enable the rapid development of antivirals for a wide variety of human pathogens, both known and newly identified, with substantial implications for the diagnosis and treatment of infectious diseases.

STAR★METHODS

Detailed methods are provided in the online version of this paper and include the following:

- KEY RESOURCES TABLE
- LEAD CONTACT AND MATERIALS AVAILABILITY
- EXPERIMENTAL MODEL AND SUBJECT DETAILS
  - Competent *E. coli*
  - Cell culture
- METHOD DETAILS
  - General Experimental Protocols and Analysis
  - CRISPR RNA Design and Viral Genome Analysis
  - Specific Experimental Protocols and Analysis
- QUANTIFICATION AND STATISTICAL ANALYSIS
- DATA AND CODE AVAILABILITY

SUPPLEMENTAL INFORMATION

Supplemental Information can be found online at https://doi.org/10.1016/j.molcel.2019.09.013.

ACKNOWLEDGMENTS

We thank J. de la Torre for providing the BHK-21 cell line and rLCMV-GFP viral stocks, protocols, and thoughtful discussions and reading of the manuscript. We thank D. Lingwood and M. Sangesland for providing the MDCK cell line and IAV viral stocks and protocols. We thank S. Whelan and L. Gehrke for providing rVSV-GFP viral stocks, BsrT7 cell line, and protocols. We thank M. Tabebordbar, A. Piantadosi, K. Barnes, K. Siddle, S. Wohl, E. Brown, and other Sabeti lab members for discussions and thoughtful manuscript feedback. Funding was provided from HHMI, NIH grant U19AI110818, and Defense Advanced Research Projects Agency (DARPA) grant D18AC00006. The views, opinions, and/or findings expressed should not be interpreted as representing the official views or policies of the Department of Defense or the US government. This study has been approved for public release; distribution is unlimited. F.Z. is supported by NIH grants 1R01-HG009761, 1R01-MH110049, and 1DP1-HL141201; HHMI; the New York Stem Cell, Allen, and Vallee foundations; the Tan-Yang Center at MIT; and J. and P. Poitras and R. Metcalfe. F.Z. is a New York Stem Cell Foundation-Robertson Investigator. All data are available in the article or the supplemental materials.

AUTHOR CONTRIBUTIONS

C.A.F. and C.M. conceived the study and wrote the paper. P.C.S. supervised the study (with assistance from N.L.Y.). C.A.F., C.M., C.K.B., A.E.L., N.L.W., A.C., and C.Y.L. performed experiments and data analysis. H.C.M. developed the crRNA target site search software. O.O.A. and J.S.G. designed transfection protocols and provided reagents and technical assistance (supervised by F.Z.). All authors reviewed the manuscript.

DECLARATION OF INTERESTS

C.A.F., C.M., P.C.S., O.O.A., J.S.G., and F.Z. are co-inventors on patent applications filed by the Broad Institute relating to work in this study. O.O.A., J.S.G., F.Z., and P.C.S. are co-founders of Sherlock Biosciences. F.Z. is a cofounder and advisor of Beam Therapeutics. O.O.A. and J.S.G. are advisors for Beam Therapeutics.

Received: April 16, 2019
Revised: July 18, 2019
Accepted: September 6, 2019
Published: October 10, 2019

REFERENCES

Abudayyeh, O.O., Gootenberg, J.S., Konermann, S., Joung, J., Slaymaker, I.M., Cox, D.B.T., Shmakov, S., Makarova, K.S., Semenova, E., Minakhin, L., et al. (2016). C2c2 is a single-component programmable RNA-guided RNA-targeting CRISPR effector. Science *353*, aaf5573.

Abudayyeh, O.O., Gootenberg, J.S., Essletzbichler, P., Han, S., Joung, J., Belanto, J.J., Verdine, V., Cox, D.B.T., Kellner, M.J., Regev, A., et al. (2017). RNA targeting with CRISPR-Cas13. Nature *550*, 280–284.

Abudayyeh, O.O., Gootenberg, J.S., Franklin, B., Koob, J., Kellner, M.J., Ladha, A., Joung, J., Kirchgatterer, P., Cox, D.B.T., and Zhang, F. (2019). A cytosine deaminase for programmable single-base RNA editing. Science *365*, 382–386.

Adiconis, X., Borges-Rivera, D., Satija, R., DeLuca, D.S., Busby, M.A., Berlin, A.M., Sivachenko, A., Thompson, D.A., Wysoker, A., Fennell, T., et al. (2013). Comparative analysis of RNA sequencing methods for degraded or low-input samples. Nat. Methods *10*, 623–629.

Aman, R., Mahas, A., Butt, H., Aljedaani, F., and Mahfouz, M. (2018a). Engineering RNA virus interference via the CRISPR/Cas13 machinery in Arabidopsis. Viruses *10*, E732.

Aman, R., Ali, Z., Butt, H., Mahas, A., Aljedaani, F., Khan, M.Z., Ding, S., and Mahfouz, M. (2018b). RNA virus interference via CRISPR/Cas13a system in plants. Genome Biol. *19*, 1.

Andersen, K.G., Shapiro, B.J., Matranga, C.B., Sealfon, R., Lin, A.E., Moses, L.M., Folarin, O.A., Goba, A., Odia, I., Ehiane, P.E., et al.; Viral Hemorrhagic Fever Consortium (2015). Clinical sequencing uncovers origins and evolution of Lassa virus. Cell *162*, 738–750.

Balish, A.L., Katz, J.M., and Klimov, A.I. (2013). Influenza: propagation, quantification, and storage. Curr. Protoc. Microbiol. *29*, 15G.1.1–15G.1.24.

Bawage, S.S., Tiwari, P.M., and Santangelo, P.J. (2018). Synthetic mRNA expressed Cas13a mitigates RNA virus infections. bioRxiv. https://doi.org/10.1101/370460.

Bolger, A.M., Lohse, M., and Usadel, B. (2014). Trimmomatic: a flexible trimmer for Illumina sequence data. Bioinformatics *30*, 2114–2120.

Brister, J.R., Ako-Adjei, D., Bao, Y., and Blinkova, O. (2015). NCBI viral genomes resource. Nucleic Acids Res. *43*, D571–D577.

Buchholz, U.J., Finke, S., and Conzelmann, K.K. (1999). Generation of bovine respiratory syncytial virus (BRSV) from cDNA: BRSV NS2 is not essential for virus replication in tissue culture, and the human RSV leader region acts as a functional BRSV genome promoter. J. Virol. *73*, 251–259.

Busan, S., and Weeks, K.M. (2018). Accurate detection of chemical modifications in RNA by mutational profiling (MaP) with ShapeMapper 2. RNA *24*, 143–148.

Cox, D.B.T., Gootenberg, J.S., Abudayyeh, O.O., Franklin, B., Kellner, M.J., Joung, J., and Zhang, F. (2017). RNA editing with CRISPR-Cas13. Science *358*, 1019–1027.

De Clercq, E., and Li, G. (2016). Approved antiviral drugs over the past 50 years. Clin. Microbiol. Rev. *29*, 695–747.

Dirks, R.M., Bois, J.S., Schaeffer, J.M., Winfree, E., and Pierce, N.A. (2007). Thermodynamic analysis of interacting nucleic acid strands. SIAM Rev. *49*, 65–88.

East-Seletsky, A., O'Connell, M.R., Knight, S.C., Burstein, D., Cate, J.H.D., Tjian, R., and Doudna, J.A. (2016). Two distinct RNase activities of CRISPR-C2c2 enable guide-RNA processing and RNA detection. Nature *538*, 270–273.

Geisbert, T.W. (2018). Predicting outcome and improving treatment for Lassa fever. Lancet Infect. Dis. *18*, 594–595.

Gootenberg, J.S., Abudayyeh, O.O., Lee, J.W., Essletzbichler, P., Dy, A.J., Joung, J., Verdine, V., Donghia, N., Daringer, N.M., Freije, C.A., et al. (2017). Nucleic acid detection with CRISPR-Cas13a/C2c2. Science *356*, 438–442.

Gootenberg, J.S., Abudayyeh, O.O., Kellner, M.J., Joung, J., Collins, J.J., and Zhang, F. (2018). Multiplexed and portable nucleic acid detection platform with Cas13, Cas12a, and Csm6. Science *360*, 439–444.

Hoffmann, E., Neumann, G., Kawaoka, Y., Hobom, G., and Webster, R.G. (2000). A DNA transfection system for generation of influenza A virus from eight plasmids. Proc. Natl. Acad. Sci. USA *97*, 6108–6113.

Katoh, K., and Standley, D.M. (2013). MAFFT multiple sequence alignment software version 7: improvements in performance and usability. Mol. Biol. Evol. *30*, 772–780.

Kim, S., Kim, D., Cho, S.W., Kim, J., and Kim, J.-S. (2014). Highly efficient RNA-guided genome editing in human cells via delivery of purified Cas9 ribonucleoproteins. Genome Res. *24*, 1012–1019.

Konermann, S., Lotfy, P., Brideau, N.J., Oki, J., Shokhirev, M.N., and Hsu, P.D. (2018). Transcriptome engineering with RNA-targeting type VI-D CRISPR effectors. Cell *173*, 665–676.e14.

Liu, X., Hao, R., Chen, S., Guo, D., and Chen, Y. (2015). Inhibition of hepatitis B virus by the CRISPR/Cas9 system via targeting the conserved regions of the viral genome. J. Gen. Virol. *96*, 2252–2261.

Low, J.T., Knoepfel, S.A., Watts, J.M., ter Brake, O., Berkhout, B., and Weeks, K.M. (2012). SHAPE-directed discovery of potent shRNA inhibitors of HIV-1. Mol. Ther. *20*, 820–828.

Ma, Z., Zhu, P., Shi, H., Guo, L., Zhang, Q., Chen, Y., Chen, S., Zhang, Z., Peng, J., and Chen, J. (2019). PTC-bearing mRNA elicits a genetic compensation response via Upf3a and COMPASS components. Nature *568*, 259–263.

Marsh, G.A., Hatami, R., and Palese, P. (2007). Specific residues of the influenza A virus hemagglutinin viral RNA are important for efficient packaging into budding virions. J. Virol. *81*, 9727–9736.

Mathews, D.H., Sabina, J., Zuker, M., and Turner, D.H. (1999). Expanded sequence dependence of thermodynamic parameters provides improved prediction of RNA secondary structure. J. Mol. Biol. *288*, 911–940.

Matranga, C.B., Andersen, K.G., Winnicki, S., Busby, M., Gladden, A.D., Tewhey, R., Stremlau, M., Berlin, A., Gire, S.K., England, E., et al. (2014). Enhanced methods for unbiased deep sequencing of Lassa and Ebola RNA viruses from clinical and biological samples. Genome Biol. *15*, 519.

Myhrvold, C., Freije, C.A., Gootenberg, J.S., Abudayyeh, O.O., Metsky, H.C., Durbin, A.F., Kellner, M.J., Tan, A.L., Paul, L.M., Parham, L.A., et al. (2018). Field-deployable viral diagnostics using CRISPR-Cas13. Science *360*, 444–448.

Ngo, N., Henthorn, K.S., Cisneros, M.I., Cubitt, B., Iwasaki, M., de la Torre, J.C., and Lama, J. (2015). Identification and mechanism of action of a novel small-molecule inhibitor of arenavirus multiplication. J. Virol. *89*, 10924–10933.

Ophinni, Y., Inoue, M., Kotaki, T., and Kameoka, M. (2018). CRISPR/Cas9 system targeting regulatory genes of HIV-1 inhibits viral replication in infected T-cell cultures. Sci. Rep. *8*, 7784.

Pédelacq, J.-D., Cabantous, S., Tran, T., Terwilliger, T.C., and Waldo, G.S. (2006). Engineering and characterization of a superfolder green fluorescent protein. Nat. Biotechnol. *24*, 79–88.

Perez, M., and de la Torre, J.C. (2003). Characterization of the genomic promoter of the prototypic arenavirus lymphocytic choriomeningitis virus. J. Virol. *77*, 1184–1194.

Price, A.A., Sampson, T.R., Ratner, H.K., Grakoui, A., and Weiss, D.S. (2015). Cas9-mediated targeting of viral RNA in eukaryotic cells. Proc. Natl. Acad. Sci. USA *112*, 6164–6169.

Raabe, V., and Koehler, J. (2017). Laboratory diagnosis of Lassa fever. J. Clin. Microbiol. *55*, 1629–1637.

Ramanan, V., Shlomai, A., Cox, D.B.T., Schwartz, R.E., Michailidis, E., Bhatta, A., Scott, D.A., Zhang, F., Rice, C.M., and Bhatia, S.N. (2015). CRISPR/Cas9 cleavage of viral DNA efficiently suppresses hepatitis B virus. Sci. Rep. *5*, 10833.

Roehm, P.C., Shekarabi, M., Wollebo, H.S., Bellizzi, A., He, L., Salkind, J., and Khalili, K. (2016). Inhibition of HSV-1 replication by gene editing strategy. Sci. Rep. *6*, 23146.

Salvato, M.S., and Shimomaye, E.M. (1989). The completed sequence of lymphocytic choriomeningitis virus reveals a unique RNA structure and a gene for a zinc finger protein. Virology *173*, 1–10.

Sánchez, A.B., and de la Torre, J.C. (2006). Rescue of the prototypic Arenavirus LCMV entirely from plasmid. Virology *350*, 370–380.

Schott, D.H., Cureton, D.K., Whelan, S.P., and Hunter, C.P. (2005). An antiviral role for the RNA interference machinery in Caenorhabditis elegans. Proc. Natl. Acad. Sci. USA *102*, 18420–18424.

Schulze, I.T., and Schlesinger, R.W. (1963). Plaque assay of dengue and other group B arthropod-borne viruses under methyl cellulose overlay media. Virology *19*, 40–48.

Shmakov, S., Abudayyeh, O.O., Makarova, K.S., Wolf, Y.I., Gootenberg, J.S., Semenova, E., Minakhin, L., Joung, J., Konermann, S., Severinov, K., et al. (2015). Discovery and functional characterization of diverse class 2 CRISPR-Cas systems. Mol. Cell *60*, 385–397.

Siegfried, N.A., Busan, S., Rice, G.M., Nelson, J.A.E., and Weeks, K.M. (2014). RNA motif discovery by SHAPE and mutational profiling (SHAPE-MaP). Nat. Methods *11*, 959–965.

Strecker, J., Jones, S., Koopal, B., Schmid-Burgk, J., Zetsche, B., Gao, L., Makarova, K.S., Koonin, E.V., and Zhang, F. (2019). Engineering of CRISPR-Cas12b for human genome editing. Nat. Commun. *10*, 212.

Strutt, S.C., Torrez, R.M., Kaya, E., Negrete, O.A., and Doudna, J.A. (2018). RNA-dependent RNA targeting by CRISPR-Cas9. eLife *7*, e32724.

Sullivan, B.M., Emonet, S.F., Welch, M.J., Lee, A.M., Campbell, K.P., de la Torre, J.C., and Oldstone, M.B. (2011). Point mutation in the glycoprotein of lymphocytic choriomeningitis virus is necessary for receptor binding, dendritic cell infection, and long-term persistence. Proc. Natl. Acad. Sci. USA *108*, 2969–2974.

Tang, M.W., and Shafer, R.W. (2012). HIV-1 antiretroviral resistance: scientific principles and clinical applications. Drugs *72*, e1–e25.

Tomkins-Tinch, C., Ye, S., Metsky, H., Jungreis, I., Sealfon, R., Yang, X., Anderson, K., Lin, M., and Park, D. (2017). Broad institute viral-ngs: v1.15.3. https://github.com/broadinstitute/viral-ngs/releases/tag/v1.15.3.

van Hemert, F., van der Kuyl, A.C., and Berkhout, B. (2016). Impact of the biased nucleotide composition of viral RNA genomes on RNA structure and codon usage. J. Gen. Virol. *97*, 2608–2619.

von Eije, K.J., ter Brake, O., and Berkhout, B. (2008). Human immunodeficiency virus type 1 escape is restricted when conserved genome sequences are targeted by RNA interference. J. Virol. *82*, 2895–2903.

Wang, Z., Wang, W., Cui, Y.C., Pan, Q., Zhu, W., Gendron, P., Guo, F., Cen, S., Witcher, M., and Liang, C. (2018). HIV-1 employs multiple mechanisms to resist Cas9/single guide RNA targeting the viral primer binding site. J. Virol. *92*, e01135-18.

Westerhout, E.M., Ooms, M., Vink, M., Das, A.T., and Berkhout, B. (2005). HIV-1 can escape from RNA interference by evolving an alternative structure in its RNA genome. Nucleic Acids Res. *33*, 796–804.

Wilson, R.C., and Gilbert, L.A. (2018). The promise and challenge of in vivo delivery for genome therapeutics. ACS Chem. Biol. *13*, 376–382.

Woolhouse, M.E.J., and Adair, K. (2013). The diversity of human RNA viruses. Future Virol. *8*, 159–171.

Woolhouse, M.E.J., Brierley, L., McCaffery, C., and Lycett, S. (2016). Assessing the epidemic potential of RNA and DNA viruses. Emerg. Infect. Dis. *22*, 2037–2044.

Wright, A.V., Nuñez, J.K., and Doudna, J.A. (2016). Biology and applications of CRISPR systems: harnessing nature's toolbox for genome engineering. Cell *164*, 29–44.

Yang, X., Charlebois, P., Macalalad, A., Henn, M.R., and Zody, M.C. (2013). V-Phaser 2: variant inference for viral populations. BMC Genomics *14*, 674.

Yin, C., Zhang, T., Qu, X., Zhang, Y., Putatunda, R., Xiao, X., Li, F., Xiao, W., Zhao, H., Dai, S., et al. (2017). In vivo excision of HIV-1 provirus by saCas9 and multiplex single-guide RNAs in animal models. Mol. Ther. *25*, 1168–1186.

Zadeh, J.N., Steenberg, C.D., Bois, J.S., Wolfe, B.R., Pierce, M.B., Khan, A.R., Dirks, R.M., and Pierce, N.A. (2011). NUPACK: Analysis and design of nucleic acid systems. J. Comput. Chem. *32*, 170–173.

Zhao, X., Liu, L., Lang, J., Cheng, K., Wang, Y., Li, X., Shi, J., Wang, Y., and Nie, G. (2018). A CRISPR-Cas13a system for efficient and specific therapeutic targeting of mutant KRAS for pancreatic cancer treatment. Cancer Lett. *431*, 171–181.

STAR★METHODS

KEY RESOURCES TABLE

REAGENT or RESOURCE	SOURCE	IDENTIFIER
Bacterial and Virus Strains		
Escherichia coli Endura chemically competent cells	Lucigen	Cat# 60242-2
Escherichia coli 10-beta competent cells (high efficiency)	New England Biolabs	Cat# C3019H
Stbl3 competent cells	This manuscript	N/A
rLCMV/WT (Armstrong strain)	Dr. de la Torre laboratory; Sánchez and de la Torre, 2006	N/A
IAV (A/Puerto Rico/8/1934 (H1N1))	Dr. Lingwood laboratory; Hoffmann et al., 2000.	N/A
rVSV-GFP	Dr. Whelan laboratory: Schott et al., 2005.	N/A
rLCMV/GFP-P2A-NP (Armstrong strain)	Dr. de la Torre laboratory; Ngo et al., 2015	N/A
rLCMV/GFP-P2A-NP (Clone 13 strain)	Dr. de la Torre laboratory; Ngo et al., 2015	N/A
Chemicals, Peptides, and Recombinant Proteins		
Terrific Broth Complete	Teknova	Cat# T7060-06
Dulbecco's Modified Eagle Medium with high glucose, GlutaMAX™, 25 mM HEPES	Thermo Fisher Scientific	Cat# 10564011
MEM Non-essential amino acids (100×)	Thermo Fisher Scientific	Cat# 11140076
Sodium pyruvate (100 mM)	Thermo Fisher Scientific	Cat# 11360070
Penicillin Streptomycin (10,000 U/mL)	Thermo Fisher Scientific	Cat# 15-140-122
Fetal Bovine Serum, certified, One Shot	Thermo Fisher Scientific	Cat# A3160402
Ham's F-12K Medium	Thermo Fisher Scientific	Cat# 21127022
Methyl cellulose	Sigma-Aldrich	Cat# 94378
DMEM, powder, high glucose, pyruvate	Thermo Fisher Scientific	Cat# 12800082
Sodium bicarbonate	Sigma-Aldrich	Cat# S5761
Methylene blue	Sigma-Aldrich	Cat# M9140
Methanol	VWR	Cat# BDH1135-1LP
Bovine Albumin Fraction V (7.5% solution)	Thermo Fisher Scientific	Cat# 15260037
Trypsin, TPCK treated	Thermo Fisher Scientific	Cat# 20233
Q5 Hot Start High-Fidelity DNA polymerase	New England Biolabs	Cat# M0493
EcoRI-HF	New England Biolabs	Cat# R3101
Gibson Assembly Master Mix	New England Biolabs	Cat# E2611
T4 DNA ligase reaction buffer	New England Biolabs	Cat# B0202
T4 Polynucleotide Kinase	New England Biolabs	Cat# M0201
T7 DNA ligase	New England Biolabs	Cat# M0318
BpiI (BbsI) (10 U/uL)	Thermo Fisher Scientific	Cat# ER1012
Lipofectamine 2000	Thermo Fisher Scientific	Cat# 11668019
Opti-MEM I Reduced Serum Media	Thermo Fisher Scientific	Cat# 31985088
Anhydrous citric acid	VWR	Cat# SAFS27487
Trisodium citrate dihydrate	Sigma-Aldrich	Cat# S1804
KCl	Thermo Fisher Scientific	Cat# AM9640G
Bond-Breaker TCEP Solution, Neutral pH	Thermo Fisher Scientific	Cat# 77720
0.5M EDTA	Thermo Fisher Scientific	Cat# AM9260G
Buffer P1	QIAgen	Cat# 19051

(*Continued on next page*)

Continued

REAGENT or RESOURCE	SOURCE	IDENTIFIER
Buffer P2	QIAgen	Cat# 19052
Buffer N3	QIAgen	Cat# 19064
Buffer PB	QIAgen	Cat# 19066
Buffer PE	QIAgen	Cat# 19065
RNase A	QIAgen	Cat# 19101
SuperScript III	Thermo Fisher Scientific	Cat# 18080044
Q5 Hot Start High-Fidelity 2× Master Mix	New England Biolabs	Cat# M0494
TURBO DNase	Thermo Fisher Scientific	Cat# AM2238
RNAClean XP beads	Beckman Coulter	Cat# A63987
HEPES	Thermo Fisher Scientific	Cat# 15-630-080
NaCl	Thermo Fisher Scientific	Cat# AM9760G
$MgCl_2$	Thermo Fisher Scientific	Cat# AM9530G
N-methylisatoic anhydride (NMIA)	Sigma Aldrich	Cat# 129887
DMSO	Sigma Aldrich	Cat# D5879
FastAP phosphatase	Thermo Fisher Scientific	Cat# EF0651
T4 RNA ligase 2, truncated KQ	New England Biolabs	Cat# M0373
RtcB ligase	New England Biolabs	Cat# M0458
SuperScript II	Thermo Fisher Scientific	Cat# 18064014
Manganese (II) Chloride	Sigma Aldrich	Cat# M1787
Purified *Lwa*Cas13a	Genscript	N/A
Purified *Psm*Cas13b	Genscript	N/A
Tris-HCl (pH 7.5)	Thermo Fisher Scientific	Cat# 15567027
50% glycerol solution	Teknova	Cat# G1800
USB Dithiothreitol (DTT)	Thermo Fisher Scientific	Cat# 707265ML
Murine RNase inhibitor	Thermo Fisher Scientific	Cat# M0314
NxGen T7 RNA polymerase	Lucigen	Cat# 30223-2
Ribonucleotide Solution Set	New England Biolabs	Cat# N0450
RNaseAlert QC System v2	Thermo Fisher Scientific	Cat# 4479769
Hybridase Thermostable RNase H	Epicenter	Cat# H39500
Rnase-free DNase	QIAgen	Cat# 79254
SuperScript IV	Thermo Fisher Scientific	Cat# 18090050
Random primers (hexamer)	Thermo Fisher Scientific	Cat# 48190-011
SUPERase In RNase Inhibitor	Thermo Fisher Scientific	Cat# AM2696
E. coli DNA polymerase I	New England Biolabs	Cat# M0209
E. coli DNA ligase	New England Biolabs	Cat# M0205
E. coli Rnase H	New England Biolabs	Cat# M0297
10× NEB Second Strand Buffer	New England Biolabs	Cat# B6117
10 mM dNTPs	New England Biolabs	Cat# N0447
Critical Commercial Assays		
MycoAlert™ Mycoplasma Detection Kit	Lonza	Cat# LT07-218
Q5 Site-Directed Mutagenesis Kit	New England Biolabs	Cat# E0554
Macherey-Nagel NucleoBond Extra Midi kit	Takara Bio	Cat# 740410.50
Power SYBR® Green RNA-to-CT 1-Step Kit	Thermo Fisher Scientific	Cat# 4389986
CellTiter-Glo 2.0 Assay Kit	Promega	Cat# G9242
BioLux *Gaussia* Luciferase Assay Kit	New England Biolabs	Cat# E3300
BioLux *Cypridina* Luciferase Assay Kit	New England Biolabs	Cat# E3309
Pierce *Gaussia* Luciferase Flash Assay Kit	Thermo Fisher Scientific	Cat# 16159
Pierce *Cypridina* Luciferase Flash Assay Kit	Thermo Fisher Scientific	Cat# 16169

(*Continued on next page*)

Continued

REAGENT or RESOURCE	SOURCE	IDENTIFIER
RNeasy Mini Kit	QIAgen	Cat# 74104
Zero Blunt TOPO Cloning Kit	Thermo Fisher Scientific	Cat# K280020
Illumina MiSeq 300v2	Illumina	Cat# MiSeq 300v2
MEGAscript T7 Transcription Kit	Thermo Fisher Scientific	Cat# AM1333
RNA 6000 Nano Kit	Agilent	Cat# 5067-1511
TwistAmp Basic RT	TwistDx	Cat# TABARTS01kit
QIAamp Viral RNA Mini Kit	QIAgen	Cat# 52904
Nextera XT DNA library preparation kit	Illumina	Cat# FC-131-1096
KAPA library quantification kit	Roche	Cat# KK4824
Deposited Data		
Metagenomic and LCMV sequencing reads from virus-containing supernatant (BioProject: PRJNA560406)	This manuscript	https://www.ncbi.nlm.nih.gov/bioproject/560406
Experimental Models: Cell Lines		
HEK293FT cells	American Type Culture Collection (ATCC)	Cat# PTA-5077
MDCK cells	ATCC	Cat# PTA-6500
A549 cells	ATCC	Cat# CCL-185
BHK-21 cells	ATCC	Cat# CCL-10
Vero cells	ATCC	Cat# CCL-81
BsrT7 cells	Dr. Whelan laboratory; Buchholz et al., 1999	N/A
Oligonucleotides		
Primers for cloning *Lwa*Cas13a-NES-BFP	This manuscript	Table S6
Primers for cloning *Psp*Cas13b-NLS	This manuscript	Table S6
*Lwa*Cas13a and *Psp*Cas13b spacer oligos	This manuscript	Table S6
Primers for cloning shRNA backbone plasmid	This manuscript	Table S6
shRNA oligos	This manuscript	Table S6
CRISPR array oligos	This manuscript	Table S6
Primer for LCMV RT-qPCR (forward): CAGCCAACAACTCCCACCAT	This manuscript	N/A
Primer for LCMV RT-qPCR (reverse): GAAGGCAGAGGTCAGATTGCA	This manuscript	N/A
Primer for IAV RT-qPCR (forward): CAAGCAGCAGAGGCCATGGA	Marsh et al., 2007.	N/A
Primer for IAV RT-qPCR (reverse): GACCAGCACTGGAGCTAGGA	Marsh et al., 2007.	N/A
Primer for VSV RT-qPCR (forward): TGATACAGTACAATTATTTTGGGAC	This manuscript	N/A
Primer for VSV RT-qPCR (reverse): GAGACTTTCTGTTACGGGATCTGG	This manuscript	N/A
Primers for cloning of LCMV segments analyzed by SHAPE-MaP	This manuscript	Table S8
RPA primers	This manuscript	Table S6
*Lwa*Cas13a and *Psm*Cas13b crRNAs	This manuscript	Table S6
Reporter oligos	This manuscript	Table S6
rRNA probes	Adiconis et al., 2013.	N/A
Recombinant DNA		
Plasmid: *Lwa*Cas13a-NES-GFP	Abudayyeh et al., 2017.	Addgene #105815
Plasmid: *Psp*Cas13b-NES	Cox et al., 2017	Addgene #103862

(*Continued on next page*)

Continued

REAGENT or RESOURCE	SOURCE	IDENTIFIER
Plasmid: *Lwa*Cas13a-NES-BFP	This manuscript	N/A
Plasmid: d*Lwa*Cas13a-NES-GFP	Abudayyeh et al., 2017.	N/A
Plasmid: d*Lwa*Cas13a-NLS-GFP	Abudayyeh et al., 2017.	N/A
Plasmid: *Lwa*Cas13a-NLS-GFP	Abudayyeh et al., 2017.	N/A
Plasmid: PspCas13b-NLS	This manuscript	N/A
Plasmid: LwaCas13a crRNA backbone	Abudayyeh et al., 2017.	Addgene #91906
Plasmid: PspCas13b crRNA backbone	Cox et al., 2017	Addgene #103854
Plasmid: shRNA backbone	This manuscript	N/A
Plasmid: *Gaussia-Cypridina* dual luciferase	Abudayyeh et al., 2017.	N/A
Plasmid: pCR4-TOPO/LCMV-GFP_S-NoEnds	This manuscript	N/A
Software and Algorithms		
Mafft v7.31	Katoh and Standley, 2013.	https://mafft.cbrc.jp/alignment/software/
NUPACK	Dirks et al., 2007; Zadeh et al., 2011	http://www.nupack.org/
viral-ngs v1.15.3	Tomkins-Tinch et al., 2017	https://github.com/broadinstitute/viral-ngs
Trimmomatic	Bolger et al., 2014	http://www.usadellab.org/cms/?page=trimmomatic
Shapemapper2	Busan and Weeks, 2018	https://github.com/Weeks-UNC/shapemapper2
V-Phaser2	Yang et al., 2013	https://github.com/broadinstitute/viral-ngs/blob/master/tools/vphaser2.py
Other		
BD BioCoat Clear Poly-D-Lysine 96-well microplates	Corning	Cat# 356461
BioCoat Poly-D-Lysine 96 well Black/Clear Flat Bottom, TC-treated	Corning	Cat# 356640
96-well Solid Plates, Corning, Nonbinding, Flat Bottom, White	VWR	Cat# 33501-810
96-well Filter Plate	Epoch Life Sciences	Cat# 2020-001
AirPore Tape Sheets	QIAgen	Cat# 19571
Corning 384-well Low Volume Plates, Nonsterile	VWR	Cat# 89089-862

LEAD CONTACT AND MATERIALS AVAILABILITY

Further information for most resources and reagents should be directed to and will be fulfilled by the Lead Contact, Cameron Myhrvold (cmyhrvol@broadinstitute.org). Further information for specific cell lines and viral stocks donated by other laboratories should be directed to the specific laboratory from which the original stocks were received. The authors plan to make the reagents widely available to the academic community, but some reagents may be subject to material transfer agreements.

EXPERIMENTAL MODEL AND SUBJECT DETAILS

Competent *E. coli*

Endura (Lucigen), New England Biosciences (NEB) 10-beta, and stbl3 competent *E. coli* were transformed and grown according to manufacturer's instructions. *E. coli* were plated on lysogeny broth (LB) agar plates with the appropriate antibiotic and grown at 37°C overnight. Single colonies were picked from LB agar plates and grown in Terrific Broth (TB) (Teknova) with the appropriate antibiotic and grown overnight at 37°C for plasmid production.

Cell culture

All experiments evaluating Cas13 activity against lymphocytic choriomeningitis virus (LCMV) or vesicular stomatitis virus (VSV) were performed in HEK293FT cell line (American Type Culture Collection (ATCC)). Cells were < 30 passages, mycoplasma negative as tested by the MycoAlert™ Mycoplasma Detection Kit (Lonza), and cultured in Dulbecco's Modified Eagle Medium with high glucose, GlutaMAX™, 25 mM HEPES (Thermo Fisher Scientific) supplemented with 1× non-essential amino acid solution (Thermo Fisher Scientific), 1× sodium pyruvate (Thermo Fisher Scientific), 1× penicillin-streptomycin (Thermo Fisher Scientific), and 10% fetal bovine

serum (Thermo Fisher Scientific) (cDMEM-10% FBS). Experiments evaluating Cas13 activity against influenza A virus (IAV) were either performed in Madin-Darby Canine Kidney (MDCK) epithelial cell line (donated by the Daniel Lingwood laboratory (Ragon Institute)) or adenocarcinomic human alveolar basal epithelial (A549) cell line (donated by the Nir Hacohen laboratory (Broad Institute)). MDCK cells were cultured in cDMEM-10% FBS but without 1× sodium pyruvate. A549 cells were cultured in F-12K Medium (Thermo Fisher Scientific) supplemented with 1× penicillin-streptomycin, and 10% fetal bovine serum. All cell lines were grown in tissue culture incubators at 37°C and 5% CO_2.

METHOD DETAILS

General Experimental Protocols and Analysis

Virus propagation and titering

Wild-type LCMV Armstrong (rLCMV/WT), rLCMV-GFP-P2A-NP Armstrong, and rLCMV-GFP-P2A-NP Clone 13 strains (described previously) (Ngo et al., 2015; Sánchez and de la Torre, 2006.) were propagated in baby hamster kidney 21 (BHK-21) cells (ATCC or donated by the Juan Carlos de la Torre laboratory (Scripps Research Institute)). For viral stock propagation, BHK-21 cells at 50% or 85% confluency were inoculated at an MOI of 0.01 for 1.5 h. Cells were rocked on a shaker or manually every 15-20 min, and after 1.5 h cDMEM-10% FBS was added. Virus-containing cellular supernatant was harvested 48 hours post infection (hpi), centrifuged to remove cell debris, aliquoted, and stored at −80°C until use.

LCMV viral stocks were titered via plaque assay using Vero cells (ATCC). Vero cells were seeded in a 6-well tissue culture plate 1-2 days prior to inoculation and cultured in cDMEM-10% FBS. Viral stock was diluted via 10-fold dilutions in cDMEM-2% FBS and inoculation was performed for 1 h, rocking plate either on shaker or manually every 15 min. After 1 h, inoculation media was replaced with methylcellulose overlay media(Schulze and Schlesinger, 1963). Methylcellulose overlay media was made of equal parts methylcellulose solution and 2× cDMEM-2% FBS, filter sterilized, and stored at 4°C until use. The methylcellulose solution was prepared by combining 5 g of methylcellulose (Sigma-Aldrich) for every 250 mLs of autoclaved MilliQ water. This solution was then autoclaved and cooled overnight at room temperature while being mixed on a magnetic stir plate. cDMEM-2% FBS was prepared at 2× concentration by combining 500 mLs of autoclaved MilliQ water and DMEM powder (Thermo Fisher Scientific) according to manufacturer's instructions, and each 500 mLs was supplemented with 3.75 g of sodium bicarbonate (Sigma-Aldrich), 10 mLs penicillin-streptomycin (final 2× concentration), and 20 mLs fetal bovine serum (final 4% FBS). Plaques were counted 7-14 days post infection after fixation and staining with a mixture of 0.5% methylene blue (Sigma-Aldrich) and 70% methanol (VWR). For rLCMV-GFP, titer was confirmed in parallel by counting GFP fluorescent infection foci from 4× images collected on a Cytation 5 with microscope (BioTek Instruments).

IAV (A/Puerto Rico/8/1934(H1N1)), generated by DNA transfection described previously (Hoffmann et al., 2000), was donated by the laboratory of Daniel Lingwood and propagated and titered using a protocol adapted from previous methods (Balish et al., 2013). In brief, MDCK cells were seeded 2-3 days prior to infection until cells were 95%–100% confluent. Then, IAV viral stocks were diluted 1:1,000 in Dulbecco's Modified Eagle Medium with high glucose, GlutaMAX™, 25 mM HEPES supplemented with 7.5% Bovine Albumin Fraction V (Thermo Fisher Scientific), 1× penicillin-streptomycin and TPCK-treated trypsin (Thermo Fisher Scientific) at a final concentration of 2 μg/mL (IAV infection media). Cells were inoculated for 1 h with this viral dilution and cells were rocked on a shaker or shaken manually every 20 min. After 1 h, IAV infection media was added. Cellular supernatants were harvested 48-72 hpi when > 75% of cells were exhibiting cytopathic effect (CPE). Supernatants were then centrifuged to remove cell debris, aliquoted, and stored at −80°C until use.

IAV viral stocks were titered by $TCID_{50}$ as described previously (Balish et al., 2013). In short, MDCK cells were seeded 1-2 days prior to inoculation to allow for a full monolayer to form. IAV viral stocks were thawed on ice, diluted 1:100 followed by half-log_{10} dilutions in IAV infection media. At least 4 wells were used to observe CPE 48-72 hpi, and titers were calculated using the Reed-Muench method.

rVSV-GFP was propagated in BsrT7 cells donated by the Sean Whelan lab (Harvard University) (Buchholz et al., 1999; Schott et al., 2005). BsrT7 cells at 85% or 100% confluency were inoculated at an MOI of 3 for 1 h in serum-free media. Cells were rocked on a shaker and after 1 h cDMEM-2% FBS was added. Virus-containing cellular supernatant was harvested 24 hpi, centrifuged to remove cell debris, aliquoted, and stored at −80°C until use.

rVSV-GFP viral stocks were titered via plaque assay using Vero cells. Vero cells were seeded in a 6-well tissue culture plate 1-2 days prior to inoculation and cultured in cDMEM-10% FBS. Viral stock was diluted via 10-fold dilutions in serum-free cDMEM and inoculation was performed for 1 h, rocking plate either on shaker or manually every 15 min. After 1 h, inoculation media was replaced with methylcellulose overlay media, made as described above. Plaques were counted one day post infection after fixation and staining with a mixture of 0.5% methylene blue and 70% methanol.

Cloning of plasmids

*Lwa*Cas13a-NES-GFP plasmid (Abudayyeh et al., 2017) (AddGene #105815) and *Psp*Cas13b-NES plasmid (Cox et al., 2017) (AddGene #103862) were cloned to express BFP or an NLS signal, respectively. *Lwa*Cas13a-NES-GFP was cloned to express BFP by introducing a single mutation in GFP that changes GFP to BFP (Pédelacq et al., 2006) via PCR with Q5 hot-start high-fidelity polymerase (NEB), enzymatic digestion with EcoRI-HF (NEB) and assembly by Gibson assembly (NEB). Expression, localization, and *Lwa*Cas13a cleavage activity was confirmed via transfection, imaging, and luciferase knockdown testing (see below for details).

*Psp*Cas13b-NES plasmid was cloned to express a nuclear localization signal via PCR with Q5 hot-start high-fidelity polymerase and Gibson assembly. The change in localization signal was confirmed by Sanger sequencing (Genewiz, Inc.).

Spacer sequences were cloned into *Lwa*Cas13a or *Psp*Cas13b crRNA backbone plasmids as described previously (Abudayyeh et al., 2017; Cox et al., 2017) (AddGene #91906 and #103854, respectively). In brief, complementary single-stranded DNA (ssDNA) oligos (each at a final concentration 10 μM; from Integrated DNA Technology (IDT)) encoding the spacer sequences were annealed with T4 DNA ligase buffer (final concentration at 1× ; NEB) and 0.5 μL of T4 PNK (NEB) per 10 μL reaction. Annealing conditions were the following: 30 min at 37°C and 5 min at 95°C followed by a 5°C/min ramp to 4°C. The annealed spacer oligos (diluted 1:10) were then inserted into the crRNA backbone (final concentration of 1 ng/μL) via golden gate assembly with BbsI digestion (NEB) and T7 ligase (NEB) and 4-6 cycles of 37°C for 5 min and 16°C for 5 min. Luciferase targeting and non-targeting crRNAs used in this study were published previously (Abudayyeh et al., 2017; Cox et al., 2017).

An shRNA backbone plasmid was generated by PCR amplification of the *Lwa*Cas13a crRNA backbone plasmid removing the direct repeat sequence and circularizing the PCR product via kinase, ligase and DpnI treatment (Q5 Site-directed Mutagenesis Kit, NEB). Position-matched shRNAs were designed by selecting the internal 21 nt of the crRNA spacer sequence. shRNA sequences (ordered from IDT) were inserted into the shRNA backbone plasmid with the same protocol used for crRNA spacer cloning described above.

CRISPR arrays were generated by amplifying the full-length CRISPR array sequence via PCR of overlapping, complementary ssDNA oligos (ordered from IDT) and golden-gate cloned into the *Psp*Cas13b crRNA backbone as described above.

Plasmids used in this study are listed in Table S5. Spacers, shRNAs, CRISPR arrays, and cloning oligos used in this study are listed in Table S6.

Transfection and electroporation conditions

Plasmids encoding Cas13 effectors and crRNAs were purified from bacterial culture using the Macherey-Nagel NucleoBond Xtra Midi kit (Takara Bio). HEK293FT cells were trypsinized and cell densities were counted using a Countess II (Life Technologies).

When transfection is performed prior to either LCMV or VSV infection, ~40,000 HEK293FT cells per well were plated at the same time as transfection or ~20-30,000 cells per well ~24 h prior to transfection in 96-well poly-D-lysine-coated tissue culture plates (Corning #356461 or #356640). Transfection protocol described below.

In the pilot LCMV crRNAs (pL1-L6, pS1-S6) experiments, 150 nanograms (ng) of *Lwa*Cas13a-encoding plasmid and 200 ng of crRNA-encoding plasmid was transfected per well. Lipofectamine 2000 (Thermo Fisher Scientific) was diluted in Opti-MEM (Thermo Fisher Scientific) according to manufacturer's instructions with 50 μL of plasmid-liposome mixtures added to each well. For all *Psp*Cas13b transfections, 75 ng of *Psp*Cas13b-encoding plasmid and 100 ng of crRNA-encoding plasmid was transfected per well. For CRISPR array experiments, 175 ng of *Psp*Cas13b plasmid and 100 ng of array plasmid was transfected per well.

RT-qPCR and analysis

To determine the quantity of LCMV, IAV or VSV that replicated and were subsequently secreted from cells, we measured viral RNA levels in the supernatant of infected cell cultures. Cell culture supernatants were processed either by heat inactivation (95°C for 10 min) or using the Heating Unpurified Diagnostic Samples to Obliterate Nucleases (HUDSON) protocol (Myhrvold et al., 2018). For the HUDSON protocol, cell culture supernatants were harvested, placed on ice, and mixed with tris(2-carboxyethyl)phosphine (TCEP, Thermo Fisher Scientific, used at 100 mM final concentration) and EDTA (Thermo Fisher Scientific, 1 mM final concentration). HUDSON mixtures were then incubated at 50°C for 5 min, followed by 95°C for 5 min to inactivate nucleases and viral particles respectively. Heat inactivated products were not diluted, but HUDSON products were diluted 1:10 with nuclease-free water prior to RT-qPCR. RT-qPCR was performed using the Power SYBR® Green RNA-to-CT 1-Step Kit (Thermo Fisher Scientific) according to the manufacturer's instructions. To measure LCMV RNA, primers against the S segment were used (fwd: CAGCCAACAACTCC CACCAT; rev: GAAGGCAGAGGTCAGATTGCA, ordered from IDT). To measure IAV RNA primers against the M segment (fwd: CAAGCAGCAGAGGCCATGGA ; rev: GACCAGCACTGGAGCTAGGA, ordered from IDT), validated previously, were used (Marsh et al., 2007). To measure VSV RNA, primers against the L region were used (fwd: TGATACAGTACAATTATTTTGGGAC; rev: GAGACTTTCTGTTACGGGATCTGG, ordered from IDT). A QuantStudio 6 Flex Real-Time PCR System (Applied Biosystems) was used in all experiments, with two technical replicates for each sample. A melt curve was analyzed at the end of each experiment to confirm specific amplification.

RT-qPCR analysis was performed using the Standard Curve (SC) module of the Applied Biosystems Analysis Software. A standard curve of 1:10 dilutions of LCMV, IAV, or VSV PCR target fragments from 10^7 to 10 copies per microliter was used to quantify the number of copies of viral RNA in each replicate. The average of each sample's two technical replicates was calculated. Normalized viral RNA levels were calculated as each sample's viral RNA quantity in cp/μL, divided by the median viral RNA quantity determined by RT-qPCR of all non-targeting crRNAs from a given experiment. A two-tailed, unpaired Student's t test was used to calculate significance between viral RNA levels for each crRNA and the non-targeting crRNAs.

Assessment of cell viability

Cell seeding, transfection, and infection protocols were performed as described above, and transfection was performed prior to infection. Forty-eight hours after viral inoculation, cell viability was assessed as a measurement of ATP levels in each well using CellTiter-Glo® 2.0 Assay kit (Promega) according to manufacturer's instructions. Luminescence measurements, with a 1 s integration time as defined by the manufacturer, were taken on a Cytation 5.

GFP measurement and image analysis

All GFP fluorescence readings and all imaging was performed in black, clear bottom 96-well plates (Corning #356640). All fluorescence measurements and imaging was performed on a Cytation 5 except for GFP measurements and imaging performed for the LCMV full genome screen (details below).

GFP fluorescence readings (ex: 485, em: 528) were taken from the bottom of each well either by a single point measurement or by 9 point measurements equally spaced throughout the well. Background subtracted GFP fluorescence was calculated by subtracting the mean GFP fluorescence measured in mock transfected and mock infected wells.

Imaging was performed at 4× magnification with images of the center of each well. Focus was performed via laser-autofocus in the bright field, and the resultant focal plane was used for the other channels (GFP - ex: 469, em: 525; BFP channel - ex: 390, em: 447). Bright field, GFP, and BFP exposure was equivalent across all wells within a single time point. Images were preprocessed using Gen5 microplate reader and imager software (version 3.0.3.14 or higher, BioTek Instruments). Default settings were used to flatten the background and smooth objects. The number of cells in an image was counted using a primary mask with the following parameters: light background, threshold of 5,000, object size between 5 μm and 60 μm, splitting touching objects and filling holes in each mask. Percentage of GFP positive cells was determined by measuring the fluorescence intensity within a given cell as identified by the primary mask and cells above an average intensity of 2,000 were counted as GFP positive. Image processing and object identification thresholds were calibrated on varied cell seedings and ensuring no positive GFP counts in mock transfected and mock infected wells.

Luciferase measurement and analysis

Forty thousand cells were either plated at the same time as transfection or ~30,000 cells approximately 24 h prior to transfection in 96-well poly-D-lysine coated tissue culture plates (Corning #356461 or #356640). Plasmid transfection was performed as described above with the addition of 10 ng of plasmid encoding both *Gaussia* luciferase (Gluc) and *Cypridina* luciferase (Cluc) per well. Luciferase-targeting crRNA specifically targeted Gluc, so Cluc expression levels served as an internal control.

Cellular supernatant was collected 24 and 48 hpt and measured for Gluc and Cluc levels. Four kits were used to measure luciferase levels: BioLux® *Gaussia* and *Cypridina* Luciferase Assay Kits (NEB), and *Gaussia and Cypridina* Luciferase Flash Assay Kits (Thermo Fisher Scientific). For the BioLux® kits, supernatant was diluted 1:5 in 1× PBS while for the Thermo Fisher Flash Assay kits, supernatant was diluted 1:10. Substrate buffer mixes were prepared as per manufacturer's instructions, and measurements were made in 96 well white, opaque bottom plates (Corning #3990). Fifty μL of substrate mix was added to each well using an injector attachment on the BioTek Cytation 5 and luminescence measurement were taken immediately after addition with a 1 s integration time, as per manufacturer's instructions.

Gluc levels were normalized by Cluc expression within each well by taking the ratio of Gluc luminescence measurement divided by Cluc luminescence measurement. A two-tailed, unpaired Student's t test was used to calculate significance between normalized Gluc levels for the Gluc-targeting crRNA and the non-targeting crRNA.

CRISPR RNA Design and Viral Genome Analysis

Analysis of potential target sites in viral genomes

Viral genome neighbors were downloaded from NCBI (Brister et al., 2015) and aligned using mafft v7.31(Katoh and Standley, 2013). To identify highly conserved windows that could be Cas13 target sites, we used a sliding window over the alignment (stride of 1 nt), and counted the number of polymorphic positions in each window. We defined a polymorphic position as a position with < 95% major allele frequency. We defined a highly conserved 28 nt (for *Lwa*Cas13a) or 30 nt window (for *Psp*Cas13b) as one with $\leq$ 2 polymorphic positions, with the appropriate protospacer flanking sequence (PFS) for *Lwa*Cas13a (no PFS) or *Psp*Cas13b (5′ GK), and with less than 50% of the data missing at all sites within the window. We counted the number of highly conserved windows in each genome segment for each viral species and summed across each segment within that species. For diverse species (those with zero highly conserved windows), we used a method called ADAPT (H.C.M. and P.C.S., unpublished data) to approximate the minimum number of crRNAs required to bind to 95% of the sequences within a 28 or 30 nt window of each viral genome segment alignment, allowing for up to one mismatch between the crRNA and genome sequence, and allowing for G-U pairing. We then parsed the list of target positions output by ADAPT to determine the number of potential Cas13 target sites for each genome segment of each viral species, allowing up to one, up to two, or up to four crRNAs to bind to an individual window. A list of the number of highly conserved target windows by species is reported in Table S2.

Design of LCMV crRNAs

Six pilot *Lwa*Cas13a crRNAs were designed to target the L segment of LCMV (pL1-pL6) and 5 to target the S segment of LMCV (pS1-pS5). Secondary structure prediction was performed on ~2,000 nt windows of the L gene (1-2,000, 2,001-4,000, 4,001-end), the Z gene, ~750 nt windows of the GPC gene (1-750, 751-end), ~1,000 nt windows of the NP gene (1-1,000, 1,001-end), or the 5′ and 3′ UTRs of the L and S segments of LCMV using the NUPACK web server with the Mathews et al. (1999) energy function (Dirks et al., 2007; Zadeh et al., 2011). One crRNA was designed to target each window by selecting a 28 nt sequence with low predicted secondary structure.

Twenty-three *Psp*Cas13b crRNAs were designed to target the vRNA in the L segment of LCMV. Spacer sequences were 30 nt in length and had varying degrees of nucleotide conservation across all LCMV strains. See Table S6 for all spacer sequences.

Design of IAV crRNAs

A set of 5 *Psp*Cas13b crRNAs were designed against IAV within regions of high nucleotide conservation; spacers were 30 nt in length and near *Psp*Cas13b's 5′ GK PFS. These crRNAs target either the negative sense IAV viral genome or the positive sense RNAs which include the IAV mRNAs as well as the full-length positive sense viral RNA which is used as a template to produce new negative sense IAV viral genomic RNA. crRNAs were cloned into *Psp*Cas13b crRNA backbone plasmid as described above. See Table S6 for spacer sequences.

Design of VSV crRNAs

Ten *Psp*Cas13b crRNAs were designed to target regions of the VSV genome with high sequence conservation. Two crRNAs with a spacer sequence 30 nt in length were tested for each gene. These crRNAs target both the viral RNA and the mRNA. crRNAs were cloned into *Psp*Cas13b crRNA backbone plasmid as described above. See Table S6 for spacer sequences.

Specific Experimental Protocols and Analysis

LCMV infection conditions

HEK293FT cell growth and confluency was assessed by viewing cells at 4× or 10× magnification and used to determine viral stock dilution needed for infection. LCMV viral stock was diluted in cDMEM-2% FBS, added to the cells, and the cells were incubated for 1 h either on a shaker or shaking manually every 15 min.

For experiments where transfection was performed first, 24 h post transfection (hpt), cells were inoculated with LCMV for 1 h (MOIs listed in figure legends) and virus-containing cellular supernatants was collected 48 hpi. For experiments when transfection occurs after infection, ~30,000 HEK293FT cells per well were plated in 96-well poly-D-lysine coated tissue culture plates 24 h prior to LCMV infection and transfection was performed 24 hpi.

After 1 h of infection, inoculant was inactivated to synchronize the infection and lyse any viral particles that did not infect the cells by adding 100 μL of citrate buffer at pH 3 to cells for 30 s. Citrate buffer was prepared with final concentrations of 40 mM citrate (2.8 g of anhydrous citric acid (Sigma-Aldrich) and 1.522 g trisodium citrate dihydrate (Sigma-Aldrich) per 500 mL solution), 140 mM NaCl (Thermo Fisher Scientific), and 10 mM KCl (Thermo Fisher Scientific). Components were mixed into distilled water at room temperature for 5-10 min with a stir bar, filter sterilized, and stored at 4°C until use. Cells were then washed 3 times with cDMEM-2% FBS to remove viral RNA from the lysed inoculant and enable measurement of newly produced viral RNA at downstream post-infection time points. For a comparison of the experimental conditions and results for the viruses used in this study, see Table S4.

IAV infection conditions

Twenty-four hours post electroporation or once cells reached 60% confluence, MDCK or A549 cells were inoculated at MOI 0.01 with IAV with inoculation protocol as described above in "Virus propagation and titering" with 150 μL of viral dilution added to each well. After 1 hour of incubation, inoculum was removed and cells were washed 1× with IAV infection media and then 100 μL of IAV infection media was added to each well. Twenty-four hpi or eight hpi, cellular supernatant was collected for RT-qPCR or $TCID_{50}$, respectively. For a comparison of the experimental conditions and results for the viruses used in this study, see Table S4.

VSV infection conditions

HEK293FT cells were transfected 24 h prior to infection. Cell growth and confluency was assessed by viewing cells at 4× or 10× magnification and used to determine viral stock dilution needed for infection. VSV viral stock was diluted in serum-free cDMEM, added to the cells, and the cells were incubated for 1 h either on a shaker at an MOI of 1. After 1 h of infection, cells were then washed 4 times with cDMEM-2% FBS to remove excess rVSV-GFP and enable measurement of newly produced viral RNA at downstream post-infection time points. Virus-containing cellular supernatant was collected 48 hpi. For a comparison of the experimental conditions and results for the viruses used in this study, see Table S4.

LCMV full genome screen

We took an unbiased tiling approach for the entire S and L segment of the LCMV genome. crRNA spacers, 28 nts in length, were designed to target the coding sense and the anticoding sense for each of LCMV four genes (Z, L, GPC, NP). Coding-sense targeting crRNAs have spacers that can target the mRNAs produced by transcription, but can also target the vRNA or vcRNA depending on the gene (Figures 2A and S2A). Anticoding-sense targeting crRNAs cannot target mRNAs. Coding-sense crRNAs were spaced 50 nt apart and anticoding-sense crRNAs 150 nt apart (283 crRNAs total with 207 coding sense crRNAs and 76 anticoding sense crRNAs). A full list of spacers used in the screen can be found in Table S6.

Cloning of all 283 crRNAs was performed using a similar protocol as the pilot crRNAs, described above, with a few differences noted here. Four μL of each ssDNA oligo at 10 μM was used as input in the annealing reaction and the golden gate reactions were performed for 15 cycles. Plasmids were transformed in stbl3 chemically competent cells. Single bacterial colonies were grown on LB 22.7 × 22.7cm agar plates supplemented with carbenicillin (100 μg/mL). Single colonies were inoculated in 1.2 mL of LB supplemented with carbenicillin (100 μg/mL) in 2.2 mL deep well plates (VWR) sealed with AirPore tape sheets (QIAgen). Plasmid DNA was isolated using QIAGEN miniprep buffers at volumes specified according to manufacturer's instructions. Epoch Life Sciences 96-well filter plates (#2020-001) were used to isolate plasmid DNA.

Transfection and infection experiments of all 283 crRNAs including non-targeting controls were performed across 11 black, clear bottom poly-D-lysine coated 96-well plates (Corning #356640). Forty thousand HEK293FT cells were plated at the same time as 150 ng of a *Lwa*Cas13a-NES-BFP encoding plasmid and 200 ng of crRNA-encoding plasmid were transfected per well as described above. Twenty-four hours post transfection, cells were infected with rLMCV-GFP at an MOI of 1 for 1 h with plates shaken manually

every 15 min. Well volume was increased to 100 μL with cDMEM-2% FBS after 1 hour without a citrate wash. Forty-eight hpi, GFP fluorescence (ex:485, em:535) was measured using a DTX 880 Multimode Detection (Beckman Coulter) taking 9 point measurements equally spaced throughout each well with reads taken from the bottom of the well.

Analysis of LCMV full genome screen

GFP measurements were background corrected by subtracting the median of all GFP measurements taken in mock transfected and mock infected wells across all plates. Five of nine background-corrected measurements in GFP-expressing wells had consistent GFP signal above background and were used to calculate the median background-corrected GFP fluorescence per well. We compared each tiled crRNA to the median background-corrected GFP fluorescence observed across all non-targeting controls. A two-tailed, unpaired Student's t test was used to calculate *p* values, and *p* values were corrected for multiple testing using the Benjamini-Hochberg method. Active crRNAs were defined as those with a fold-change ≥ 2 and false discovery rate ≤ 0.05.

Nearest neighbor analysis was performed by calculating the distribution of non-redundant pairwise distances between significant coding-sense targeting sites and a simulation of matched numbers of randomly chosen coding-sense sites (n = 10,000). Coding sense clustering significance was performed by calculating the z-score and *p* value of the 50 nt bins.

Mean nucleotide identity scores of LCMV were calculated by first aligning all complete or nearly complete LCMV S segments (> 3 kb long) and L segments (> 8 kb long) deposited in the NCBI genome browser(Brister et al., 2015) which includes all strains of LCMV. We then calculated an identity score for each nucleotide in the alignments of the S and L segments (i.e., which fraction of the sequences in the alignment have the consensus nucleotide at each position in the alignment). A mean value, defined as the mean nucleotide identity score, was calculated for each sliding window (28 nt in length) along the S and L segments. We then compared the distribution of mean nucleotide identity scores between the S and L segments by performing a Wilcoxon test on the distribution of mean values.

Nucleotide U content analysis was performed by calculating the percentage of Us in 50 nt windows upstream and downstream of each spacer location and then normalized by the mean U percentage by gene. All data from the tiling screen can be found in Table S7.

Analysis of LCMV pilot and PspCas13b crRNAs

Pilot LCMV target and *Psp*Cas13b target sites designed to follow up on the results of the LCMV full genome screen were analyzed for nucleotide conservation and RNA nucleotide context. Mean nucleotide identity scores were calculated as described in above in "Analysis of LCMV full genome screen," but for the pilot target sites the identity score was calculated over the entire crRNA region, 28 nt in length, and the *Psp*Cas13b target sites region was 30 nt in length. Nucleotide U content analysis was performed for the pilot target sites by calculating the percentage of Us in 50 nt windows upstream and downstream of each spacer location. Nucleotide A content analysis was performed for the pilot target sites by calculating the percentage of As in 100 nt windows upstream and downstream of each spacer location. All data from this analysis can be found in Table S7.

In vitro *transcription of LCMV S segment RNAs*

We first cloned the LCMV S segment into a plasmid to obtain error-free DNA template. We extracted total RNA from HEK293FT cells infected with rLCMV-GFP using the RNeasy Mini Kit (QIAgen) and performed RT-PCR using primers specific for the entire LCMV S segment (sans the 5′ and 3′ RNA ends, which form a panhandle structure) and SuperScript III (Thermo Fisher Scientific) and Q5 Hot Start High-Fidelity 2× Master Mix (NEB) to minimize errors. We cloned this shortened S segment cDNA using the Zero Blunt TOPO Cloning Kit (Thermo Fisher Scientific) and screened colonies by Sanger sequencing (Genewiz, Inc.) and next-generation sequencing on a MiSeq (Illumina), resulting in the plasmid pCR4-TOPO/LCMV-GFP_S-NoEnds.

We *in vitro* transcribed 3 known LCMV S segment RNAs (viral RNA/vRNA, complementary RNA/cRNA, and GFP-NP mRNA) for secondary structure determination by SHAPE-MaP. To generate each RNA, we performed PCR on pCR4-TOPO/LCMV-GFP_S-NoEnds using primers specific for vRNA, cRNA, or GFP-NP mRNA, which also add the T7 RNA polymerase promoter sequence and the appropriate LCMV 5′ and/or 3′ ends. Then, we performed *in vitro* transcription using the MEGAscript T7 Transcription Kit (Thermo Fisher Scientific) for 6-8 h. We then removed template DNA with TURBO DNase (Thermo Fisher Scientific) and purified RNAs using RNAClean XP beads (Beckman Coulter). We verified that most RNAs were full-length or near full-length using the Agilent RNA 6000 Nano Kit on the 2100 Bioanalyzer (Agilent).

Primer sequences provided in Table S8.

SHAPE-MaP of LCMV S segment RNAs

To identify flexible and structured regions of LCMV RNAs, we performed Selective 2′-Hydroxyl Acylation analyzed by Primer Extension and Mutational Profiling (SHAPE-MaP) (Siegfried et al., 2014). The SHAPE-MaP experimental flow first involves RNA folding and modification, error-prone RT, followed by next-generation sequencing and computational analysis to predict structured regions of the RNA, based on each nucleotide's SHAPE reactivity.

We performed SHAPE-MaP on LCMV S segment vRNA, cRNA, and GFP-NP mRNA, following the original SHAPE and MaP conditions closely (Siegfried et al., 2014), but with different library construction. Per protocol, we denatured 250 ng of each RNA sample (0.19 pmol vRNA, 0.19 pmol cRNA, or 0.31 pmol GFP-NP mRNA) in 0.5× TE buffer at 95°C for 2 min, cooled on ice, and then either heat denatured again (SHAPE-MaP denatured condition) or folded at 37°C for 20 min in buffer at final concentrations of 111 mM HEPES, 111 mM NaCl, and 11 mM $MgCl_2$. We then treated RNA with final concentration of 10 mM N-methylisatoic anhydride (NMIA, SHAPE-MaP modified condition) or DMSO vehicle control (SHAPE-MaP untreated condition) at 37°C for 45 min. We quenched each reaction with H_2O and purified with RNAClean XP beads.

We deviated from the library construction (Siegfried et al., 2014) by performing simultaneous 5′ and 3′ adaptor ligation to RNA instead of random-primed RT and DNA adaptor ligation. We fragmented each RNA in 1× FastAP buffer at 94°C for 3.5 min, and end-repaired with 3.5 U FastAP phosphatase (Thermo Fisher Scientific) at 37°C for 30 min to remove 3′ cyclic phosphates, which cannot ligate. Next, we ligated adaptors to both ends of RNA in a single step. We used 200 U T4 RNA ligase 2, truncated KQ (NEB) to ligate 10 pmol RA3v2 adaptor (modified with 5′ adenylation and 3′ C3 Spacer) specifically to the 3′-OH end of RNA, and used 15 pmol RtcB ligase (NEB) to ligate 10 pmol RA5v2 adaptor (modified with 5′ phosphate and 3′ phosphate) specifically to the 5′-OH end of RNA. We performed dual ligation in 1× RtcB Reaction Buffer supplemented with 0.1 mM GTP, 1 mM $MnCl_2$, and 20% (w/v) PEG8000, at 37°C for 2 hours. We removed excess adaptors with RNAClean XP beads, and then reverse transcribed the RNA using a primer complementary to the 3′ adaptor RA3v2. We followed the MaP protocol RT conditions, including 6 mM Mn^{2+} and 200 U SuperScript II (Thermo Fisher Scientific) at 42°C for 3 h, to induce read-through and mutation at NMIA-modified bases. We indexed and PCR amplified products containing RA5v2 and RA3v2 with the TruSeq Small RNA Library Prep Kit indices (RS-200-20012, −0024, −0036). We pooled each library and sequenced to > 2 M read-mates per sample using 2 × 150 bp paired-end reads from the Illumina MiSeq Reagent Kit v2.

We demultiplexed reads with viral-ngs which can be accessed at https://github.com/broadinstitute/viral-ngs/releases/tag/v1.15.3., trimmed with Trimmomatic to remove adaptors (Bolger et al., 2014), and demultiplexed, trimmed reads were used as input for Shapemapper2 (Busan and Weeks, 2018). Shapemapper2 compares mutation rates of NMIA-modified, DMSO control, and denatured condition for each RNA, and generates SHAPE reactivity values at each nucleotide. SHAPE reactivity values were then compared to the tiled crRNA fold-change values by calculating the mean SHAPE reactivity within each 28 nt spacer sequence window and the mean reactivities of windows 50 nt upstream and downstream of the spacer binding location. SHAPE reactivity values are found in Table S8.

Cas13-cRNA RNP Testing

crRNAs were synthesized chemically by Synthego, aliquoted, and stored at −80°C. *Lwa*Cas13a and *Psm*Cas13b were expressed recombinantly and purified by Genscript and aliquoted in specific storage buffers described below. Aliquots were stored at −80°C until use, stored in the following buffers (1) *Lwa*Cas13a (600 mM NaCl, 50 mM Tris-HCl pH 7.5, 5% glycerol, 2mM DTT) and (2) *Psm*Cas13b (50 mM HEPES pH 6.8, 600 mM NaCl, 5% glycerol, 2 mM DTT).

HEK293FT cells were trypsinized and cell densities were counted using a Countess II (Life Technologies). Cells were seeded in 96-well plates (Corning #356640) at a density of 30,000 cells per well 24 h prior to transfection. To form RNP complexes, *Lwa*Cas13a or *Psm*Cas13b and the relative crRNAs were diluted in equimolar amounts in Opti-MEM media with a 10% molar excess of crRNA. Lipofectamine 2000 was diluted according to the manufacturer's instructions. This Lipofectamine / RNP mixture was mixed, incubated for 20 min at room temperature and 50 μL was added to each well. LCMV infection was performed 4 h after transfection as described above. For luciferase targeting experiments, 10 ng of a dual luciferase expression plasmid was transfected with the RNPs and luciferase was measured 24 h post transfection as described above in "Luciferase measurement and analysis."

HUDSON-SHERLOCK of LCMV

Cell culture supernatants were processed using a modified HUDSON protocol (Myhrvold et al., 2018) as described above. HUDSON products were amplified using RT-RPA (TwistDx) for 20 min at 41°C using primers indicated in Table S6. Detection reactions were performed as described, but without background RNA (Gootenberg et al., 2017). RNase Alert v2 (Thermo Fisher Scientific) was used as the reporter. Storage conditions for purified *Lwa*Cas13a as described above. In brief, detection reactions contained purified *Lwa*Cas13a (final concentration of 45 nM), crRNA targeting LCMV (final concentration of 22.5 nM) in cleavage buffer (40 mM Tris-HCl, 60 mM NaCl, 6 mM $MgCl_2$, pH 7.3) with 1 μL murine Rnase inhibitor (NEB) per 20 μL reaction and 0.6 μL T7 polymerase (Lucigen) with 1 mM rNTPs (NEB) per 20 μL reaction. Fluorescence kinetics were monitored using a monochromator with excitation at 485 nm and emission at 520 nm with a reading every 5 min for up to 3 h using a Cytation 5 microplate reader in 384-well low-volume black plates (VWR). SHERLOCK fluorescence values reported were background subtracted.

For routine quantification of LCMV viral RNA in response to Cas13 targeting, primers and crRNAs targeting the L gene of LCMV were used. Additional RPA primers and crRNAs were used to detect the F260L mutation that is associated with persistent infection in mice (Sullivan et al., 2011).

For identification of the F260L mutation, we designed a SHERLOCK assay with a pair of crRNAs: a *Lwa*Cas13a crRNA targeting the F260F allele and a *Psm*Cas13b crRNA targeting the F260L allele. Detection reactions were performed using reactions containing purified *Lwa*Cas13a and *Psm*Cas13b (each at a final concentration of 45 nM with buffer storage conditions as described above) with each of the corresponding crRNAs at a final concentration of 22.5 nM. A dual RNA reporter system consisting of a FAM polyA reporter (at 4 uM final concentration) and an ATTO647N polyU reporter (at 2 uM final concentration) was used. Detection reactions were incubated for 1 h at 37°C. Fluorescence kinetics were monitored using a monochromator with excitation at 485 nm and emission at 520 nm (for FAM) and with excitation at 630 nm and emission at 675 nm (for ATTO647N) with a reading every 5 min for 1 h using a Cytation 5 microplate reader.

All RPA primers, crRNA, and RNA reporter sequences are listed in Table S6.

IAV $TCID_{50}$ set up and analysis

$TCID_{50}$ assays were used to calculate IAV infectivity and were performed as described above in "Virus propagation and titering" with a few exceptions. Eight hours after IAV inoculation of MDCKs expressing *Psp*Cas13b and crRNA, virus-containing cellular supernatant was removed and pooled across biological replicates. The supernatant was then initially diluted 1:50 instead of a 1:100 dilution followed by half-log_{10} dilutions in IAV infection media.

Viral genome sequencing and analysis

Viral RNA was extracted from virus-containing supernatant 48 hpi using QIAamp Viral RNA Mini (QIAgen) according to the manufacturer's protocol and with carrier RNA (poly(rA)). Viral RNA was prepared for sequencing using library construction methods that have been previously described with a few differences noted below (Matranga et al., 2014). In short, following extraction, RNA was DNase treated with Turbo DNase and then carrier RNA and ribosomal RNA was depleted using 40 nt oligo(dT) probes (IDT), custom rRNA probes (Eurofins MWG Operon), of which sequences published previously (Adiconis et al., 2013), and Hybridase Thermostable RNase H (Epicenter), followed by RNase-free DNase treatment (QIAGEN). Double-stranded complementary DNA (cDNA) was constructed using random primers and SuperScript IV (Thermo FIsher Scientific) for first-strand synthesis and *E. coli* polymerase I (NEB) for second-strand synthesis. Sequencing libraries were generated using the Nextera XT DNA Library Prep Kit (Illumina) with 10-16 cycles of PCR to introduce unique dual index pairs. Libraries were then quantified using the KAPA Universal Complete Kit (Roche) and 12-18 samples were pooled for sequencing including a no input negative control. Samples were sequenced to > 0.82 M readmates using 2 × 150 bp paired-end reads from the Illumina MiSeq Reagent Kit v2. Duplicate independent sequencing libraries were made from each carrier RNA and rRNA depleted RNA sample.

Reads were demultiplexed and independent libraries were analyzed using viral-ngs which can be accessed at https://github.com/broadinstitute/viral-ngs/releases/tag/v1.15.3. Using viral-ngs, reads from human and known laboratory microbial contaminants (such as *E. coli* and *Pseudomonas fluorescens*) were removed. The consensus LCMV genome sequence of the viral population from each sample was constructed by *de novo* assembly using the LCMV reference sequences deposited on NCBI (Brister et al., 2015). SNVs were identified using V-Phaser2 (Yang et al., 2013). To distinguish true SNVs from sequencing errors, SNVs were restricted to those present in two independent sequencing libraries and without strand bias. We also filtered detected SNVs to those present at > 0.5%, since those at lower-frequency would not be confidently identified for samples at the lower end of the coverage range. Consensus sequences are included in Data S1 and details on mean coverage across the full genome, crRNA sites, and SNVs are included in Table S3.

QUANTIFICATION AND STATISTICAL ANALYSIS

Viral titers and viral infectivity were calculated either plaque assay or $TCID_{50}$ depending on the virus. Titers determined by $TCID_{50}$ were calculated using the Reed-Muench method. Viral RNA levels were quantified by RT-qPCR using the Standard Curve (SC) module of the Applied Biosystems Analysis Software. A standard curve of 1:10 dilutions of PCR target fragments from 10^7 to 10 copies per microliter was used to convert C_T values to the number of copies of viral RNA in each replicate. See Method Details section "RT-qPCR and analysis" for more details about primer sequences used for each viral target. Statistical comparisons between non-targeting and targeting crRNAs were calculated via a two-tailed, unpaired Student's t test; $p < 0.01$ denoted in red and noted in the figure legends. For the LCMV full-genome screen analysis, *p* values were corrected for multiple testing using the Benjamini-Hochberg method. Statistical tests performed for specific full genome screen analysis are described in Method Details section "Analysis of LCMV full genome screen." See Method Details section "Viral genome sequencing and analysis" for more details about the quantification of SNVs in the sequencing data from virus-containing cell culture supernatant.

DATA AND CODE AVAILABILITY

The accession number for the metagenomic and LCMV sequencing reads (cleaned of human reads) generated from the virus-containing cell culture supernatant (details described above in "Viral genome sequencing and analysis") reported in this paper is on NCBI as BioProject: PRJNA560406 (https://www.ncbi.nlm.nih.gov/bioproject/560406).